UNIVERSITÀ DEGLI STUDI DI BERGAMO
DIPARTIMENTO DI INGEGNERIA DELL'INFORMAZIONE
E METODI MATEMATICI°

QUADERNI DEL DIPARTIMENTO

Department of Information Technology and Mathematical Methods

Working Paper

Series "*Mathematics and Statistics*"

n. 6/MS – 2011

Time accurate partitioned algorithms for the solution of fluid-structure interaction problems in haemodynamics

by

F. Nobile, M. Pozzoli, C. Vergara

° Viale Marconi. 5, I – 24044 Dalmine (BG), ITALY, Tel. +39-035-2052339; Fax. +39-035-562779

[§] L'accesso alle *Series* è approvato dal Comitato di Redazione. I *Working Papers* della Collana dei Quaderni del Dipartimento di Ingegneria dell'Informazione e Metodi Matematici costituiscono un servizio atto a fornire la tempestiva divulgazione dei risultati dell'attività di ricerca, siano essi in forma provvisoria o definitiva.

Time accurate partitioned algorithms for the solution of fluid-structure interaction problems in haemodynamics*

F. Nobile[1], M. Pozzoli[1], C. Vergara[2]

July 11, 2011

[1] MOX– Modellistica e Calcolo Scientifico
Dipartimento di Matematica "F. Brioschi"
Politecnico di Milano
via Bonardi 9, 20133 Milano, Italy
fabio.nobile@polimi.it, matteo1.pozzoli@mail.polimi.it

[2] Dipartimento di Ingegneria dell'Informazione e Metodi Matematici
Università di Bergamo
via Marconi 5, 24044, Italy
christian.vergara@polimi.it

Keywords: Fluid-structure interaction, blood flow, BDF schemes, time accuracy, partitioned schemes

Abstract

In this work we deal with the numerical solution of the fluid-structure interaction problem arising in the haemodynamic environment. In particular, we consider BDF and Newmark time discretization schemes, and we study different methods for the treatment of the fluid-structure interface position, focusing on partitioned algorithms for the prescription of the continuity conditions at the fluid-structure interface. We consider explicit and implicit algorithms, and new hybrid methods. We study numerically the performances and the accuracy of these schemes, highlighting the best solutions for haemodynamic applications. We also study numerically their convergence properties with respect to time discretization, by introducing an analytical test case.

*This work has been supported by the ERC Advanced Grant N.227058 MATHCARD

1 Introduction

Building efficient strategies for the solution of the fluid-structure interaction (FSI) problem is a major issue in *computational haemodynamics*. In particular here we are interested in the FSI problem arising by the interaction between the blood flow and the vessel wall deformation (see, e.g., [1, 2, 3, 4, 5, 6]). The main difficulties related to the numerical solution of the FSI problem are:

1. the treatment of the *interface position*, since the fluid domain is an unknown of the problem (*geometrical non-linearities*);

2. the treatment of the *interface continuity conditions*, which enforce continuity of velocities and normal stresses between fluid and structure;

3. the fact that the subproblems could be non-linear (*physical non-linearities*).

These features make the FSI problem a strongly non-linear coupled problem, as there is a substantial amount of energy exchanged between fluid and structure in each cardiac beat. This non-linear behaviour is essentially related to points 1 and 2 above. Therefore, in this work we focus mainly on these two points. Regarding the third point, we consider just the fluid non-linearity due to the convective term in the Navier-Stokes equations, and we consider a linear structure. The problem of how to include efficiently the structure non-linearities in FSI algorithms will be the subject of a future work.

Concerning the first point, we can mainly detect two strategies: an *implicit treatment* of the interface position, through, for example, fixed point or Newton iterations (see, e.g., [7, 8]), or an *explicit treatment*, thanks to extrapolations of the solution at previous time steps (see, e.g., [9, 10, 11]). In the haemodynamic context, it is still not clear wheather the use of an implicit treatment of the FS interface is really needed in terms of stability and accuracy of the methods.

After a suitable linearization of the physical non-linearities, whichever of the two strategies is adopted for the treatment of the interface position (implicit or explicit), one has to deal with a *linearized* FSI problem (in the sense that we have eliminated the geometrical and physical non-linearities). However, this problem is still coupled through the interface continuity conditions. For the solution of this linearized FSI problem, two strategies have been proposed and widely studied in the literature, namely the *monolithic* and the *partitioned* approaches. In the first case, the linearized problem is solved by building the whole FSI matrix, and then by solving the related linear system with a suitable preconditioned Krylov [7, 2], domain-decomposition [12] or multigrid [13] method. Obviously, in this way the interface continuity conditions are automatically satisfied. Alternatively, in partitioned schemes one solves the fluid and structure subproblems in an iterative framework, until fulfillment of the interface continuity conditions (see, e.g., [14, 15, 16, 17, 5]. Since we are interested in developing modular algorithms, which allow the use of pre-existing fluid and structure codes, we do not consider the monolithic approach here.

The first goal of this work is to compare the accuracy and performances of different treatments of the FS interface position, when partitioned procedures are considered for the enforcement of the continuity conditions. We consider a general framework in which iterations on the interface position as well as those on the continuity conditions are performed. We study and compare several strategies, namely a "Double-loop" strategy where two nested loops are considered, a "Single-loop" strategy where only one loop is performed, and variants of these (called GCIS-m and ICIS-n) where only an *a priori* fixed number of external or internal iterations are performed. Finally, we consider the geometric explicit strategy (GCIS-1) where only one iteration on the interface position per time step is performed [10, 12]. The numerical results show that there is no significant differences between the two implicit schemes (Double-loop and Single-loop), with a slight preference for Double-loop in terms of computational cost. Moreover, they show that GCIS-m schemes for $m = 1, 2, 3$, although not guaranteeing convergence to the interface conditions at each time step, preserve a good accuracy with a significative reduction in the CPU time with respect to implicit methods.

The second goal of the paper is to develop efficient ways to build high-order temporal schemes for the solution of the FSI problem. We consider the *Newmark scheme* for the structure in combination with the *theta-method* for the fluid, and BDF schemes up to fourth order for both subproblems. In particular, we study if suitable extrapolations of the interface quantities at each time step improve the time accuracy and/or reduce the number of iterations on the interface position.

The outline of the work is as follows. In Section 2 we introduce the FSI problem, its time discretization and a Lagrange multipliers-based formulation, helpful for the derivation of the numerical schemes. In Section 3 we introduce and discuss the schemes for the numerical solution. In Section 4 we show several 3D numerical results, both in simplified and in real 3D geometries. In Section 5 we propose an analytical test case to check the convergence properties of the schemes introduced, and we show related numerical results. Finally, in Section 6 we draw some conclusions.

2 The FSI problem and its time discretization

2.1 The continuous FSI problem

Let us consider an open domain $\Omega_f^t \subset \mathbb{R}^3$ like the one represented in Figure 1 (on the left). This represents the lumen of a vessel and it is function of time t. Inflow and outflow sections are denoted by $\Sigma_{f,i}^t$ (three in Figure 1). Blood velocity is denoted by $\boldsymbol{u}_f(\boldsymbol{x}, t)$, the pressure by $p_f(\boldsymbol{x}, t)$. The incompressible Navier-Stokes equations for a Newtonian fluid are assumed to hold in Ω_f^t. Let $\boldsymbol{T}_f$ be the related Cauchy stress tensor defined by

$$\boldsymbol{T}_f(\boldsymbol{u}_f, p_f) := -p_f \boldsymbol{I} + \mu(\nabla \boldsymbol{u}_f + (\nabla \boldsymbol{u}_f)^T).$$

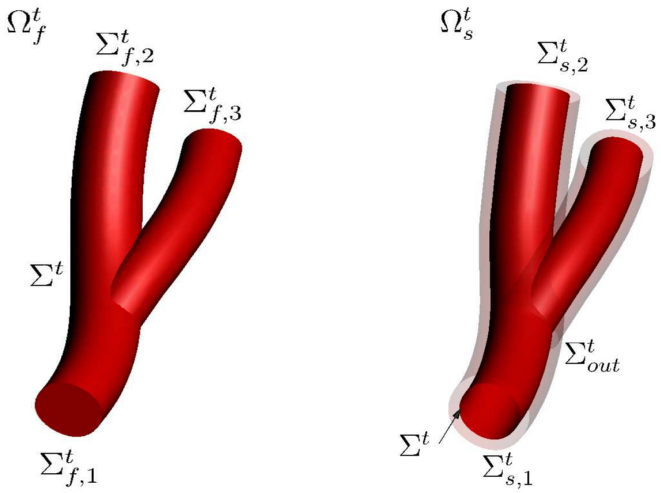

Figure 1: Representation of the domain of the FSI problem: fluid domain on the left, structure domain on the right.

Since we work in a moving domain, the fluid problem is stated in an *Arbitrary Lagrangian-Eulerian* (ALE) framework (see e.g. [18, 19]). The ALE map $\mathcal{A}$ is defined by an appropriate lifting of the structure displacement at the FS interface Σ^t, and defines the displacement of the points of the fluid domain $\boldsymbol{\eta}_m$ and their velocity $\boldsymbol{u}_m$. For any function v living in the current fluid configuration, we denote by $\widetilde{v} := v \circ \mathcal{A}$ its counterpart in the reference configuration. The ALE time derivative for a function $\boldsymbol{v}$ is defined as $\frac{D^A \boldsymbol{v}}{Dt} := \frac{\partial \widetilde{\boldsymbol{v}}}{\partial t} \circ \mathcal{A}^{-1}$, and the following identity holds

$$\frac{\partial \widetilde{\boldsymbol{v}}}{\partial t} = \frac{D^A \boldsymbol{v}}{Dt} - (\boldsymbol{u}_m \cdot \nabla)\boldsymbol{v}.$$

A classical choice in haemodynamic applications to define the ALE map is to consider a harmonic extension operator in the reference domain (see, e.g., [20]).

The vessel wall is denoted by Ω_s^t, which is an open subset of $\mathbb{R}^3$ (see Figure 1, right). The intersection of Ω_s^t and Ω_f^t is empty, and $\Sigma^t := \bar{\Omega}_s^t \cup \bar{\Omega}_f^t$ is the FS interface. On Σ^t we define a normal unit vector $\boldsymbol{n}$ poiting outward of the solid domain and inward to the fluid domain. The inflow/outflow sections (three in Figure 1) are denoted by $\Sigma_{s,i}^t$. With Σ_{out}^t we denote the external surface of the structure domain. We denote by $\boldsymbol{\eta}_s(\boldsymbol{x}, t)$ the wall displacement, and by $\boldsymbol{T}_s = \boldsymbol{T}_s(\boldsymbol{\eta}_s)$ the Cauchy stress tensor for the structure. To describe the structure kinematics we adopt a purely Lagrangian approach, where $\mathcal{L}$ is the Lagrangian map. For any function g defined in the current solid configuration Ω_s^t, we denote by $\widetilde{g} := g \circ \mathcal{L}$ its counterpart in the reference domain. With this notation, we can write the Piola-Kirchhoff stress tensor $\widetilde{\boldsymbol{T}}_s$ in terms of the

Cauchy tensor as $\widetilde{\boldsymbol{T}}_s(\widetilde{\boldsymbol{\eta}}_s) = J_s(\boldsymbol{\eta}_s)\boldsymbol{T}_s(\boldsymbol{\eta}_s)\boldsymbol{F}_s^{-T}(\boldsymbol{\eta}_s)$, where $\boldsymbol{F}_s := \nabla_{\boldsymbol{x}_s^0}\boldsymbol{x}_s^t$ is the deformation gradient with respect to the reference coordinates $\boldsymbol{x}_s^0$, $\boldsymbol{x}_s^t$ is the current coordinate, and $J_s := det(\boldsymbol{F}_s)$ is the local change of volume. The Piola-Kirchhoff stress tensor is related to the deformation gradient $\boldsymbol{F}_s$ by some linear or non-linear relation. In setting the general FSI problem we will assume an arbitrary non-linear constitutive relation. However, in describing the practical algorithms in Section 3 and in the numerical tests we will focus only on linear elastic models.

The strong formulation of the FSI problem, including the computation of the ALE map reads therefore as follows

1. *Fluid-Structure problem.* Given the (unknown) fluid domain velocity $\boldsymbol{u}_m$ and fluid domain Ω_f^t, find, at each time $t \in (0,T]$, fluid velocity $\boldsymbol{u}_f$, pressure p_f and structure displacement $\boldsymbol{\eta}_s$ such that

$$\begin{cases} \rho_f \dfrac{D^A \boldsymbol{u}_f}{Dt} + \rho_f((\boldsymbol{u}_f - \boldsymbol{u}_m)\cdot\nabla)\boldsymbol{u}_f - \nabla\cdot\boldsymbol{T}_f(\boldsymbol{u}_f, p_f) = \boldsymbol{f}_f & \text{in } \Omega_f^t, \\ \nabla\cdot\boldsymbol{u}_f = 0 & \text{in } \Omega_f^t, \\ \rho_s \dfrac{\partial^2\widetilde{\boldsymbol{\eta}}_s}{\partial t^2} + \mathcal{D}\left(\dfrac{\partial\widetilde{\boldsymbol{\eta}}_s}{\partial t}\right) - \nabla\cdot\widetilde{\boldsymbol{T}}_s(\widetilde{\boldsymbol{\eta}}_s) = \widetilde{\boldsymbol{f}}_s & \text{in } \Omega_s^0, \\ \boldsymbol{u}_f = \dfrac{\partial\boldsymbol{\eta}_s}{\partial t} & \text{on } \Sigma^t, \\ \boldsymbol{T}_s(\boldsymbol{\eta}_s)\,\boldsymbol{n} - \boldsymbol{T}_f(\boldsymbol{u}_f, p_f)\,\boldsymbol{n} = \boldsymbol{0} & \text{on } \Sigma^t, \\ \alpha_e\widetilde{\boldsymbol{\eta}}_s + \widetilde{\boldsymbol{T}}_s(\widetilde{\boldsymbol{\eta}}_s)\,\widetilde{\boldsymbol{n}} = P_{ext}\widetilde{\boldsymbol{n}}, & \text{on } \Sigma_{out}^0, \end{cases} \tag{1}$$

   where $\mathcal{D}$ is a linear dumping operator, ρ_f and ρ_s are the fluid and structure densities, μ is the constant blood viscosity, $\boldsymbol{f}_f$ and $\boldsymbol{f}_s$ the forcing terms;

2. *Geometry problem.* Given the (unknown) interface structure displacement $\widetilde{\boldsymbol{\eta}}_s|_{\Sigma^0}$, find the displacement of the points of the fluid domain $\boldsymbol{\eta}_m$ such that

$$\begin{cases} -\triangle\widetilde{\boldsymbol{\eta}}_m = \boldsymbol{0} & \text{on } \Omega_f^0, \\ \widetilde{\boldsymbol{\eta}}_m = \widetilde{\boldsymbol{\eta}}_s & \text{on } \Sigma^0, \end{cases} \tag{2}$$

   and then find accordingly the fluid domain velocity $\widetilde{\boldsymbol{u}}_m := \frac{\partial\widetilde{\boldsymbol{\eta}}_m}{\partial t}$, and the new points $\boldsymbol{x}_f^t$ of the fluid domain by moving the points $\boldsymbol{x}_f^0$ of the reference domain Ω_f^0:

$$\boldsymbol{x}_f^t = \boldsymbol{x}_f^0 + \widetilde{\boldsymbol{\eta}}_m.$$

The two matching conditions enforced at the interface are the *continuity of velocities* $(1)_4$ and the *continuity of normal stresses* $(1)_5$. The fluid and structure are also coupled by the geometry problem, leading to a highly nonlinear system of partial differential equations. Equations (1) and (2) have to be endowed with suitable boundary conditions on $\Omega_f^t \setminus \Sigma^t$ and $\Omega_s^0 \setminus (\Sigma^0 \cup \Sigma_{out}^0)$, and with suitable initial conditions. We prescribe the Robin boundary condition $(1)_6$ on Σ_{out}^0, with

the aim of modeling the presence of a surrounding tissue around the vessel. This choice corresponds to consider an elastic behaviour of this tissue, where α_e is the corresponding elastic coefficient (see [21, 22]).

2.2 Time discretization of the FSI problem

Let Δt be the time discretization parameter and $t^n := n\,\Delta t$, $n = 0, 1, \ldots$. For a generic function z, with z^n we denote the approximation of $z(t^n)$. In this work we consider two families of schemes, namely the *Backward Differentiation Formulae* (BDF) schemes (see [23, 24]) and the family obtained by the *Newmark* schemes for the structure, and the *theta-methods* for the fluid. We propose here a unified formulation of the time discrete problem (1)-(2), that accommodates both families of schemes.

1. *Fluid-Structure problem.* Given the (unknown) fluid domain velocity $\boldsymbol{u}_m^{n+1}$ and the fluid domain Ω_f^{n+1}, the parameters $\beta_{f,i} (i = 0, \ldots, p)$, χ_f, $\beta_{s,i} (i = 0, \ldots, p)$, σ_s, ζ_s, $\xi_{s,i} (i = 0, \ldots, p+1)$, χ_s, κ_s, the solution at previous time steps, and functions $\boldsymbol{f}_f^{n+1}$, $\boldsymbol{f}_s^{n+1}$ and P_{ext}, find fluid velocity $\boldsymbol{u}_f^{n+1}$, pressure p_f^{n+1} and structure displacement $\boldsymbol{\eta}_s^{n+1}$ such that

$$
\begin{cases}
\rho_f \dfrac{\beta_{f,0}}{\Delta t}\boldsymbol{u}_f^{n+1} + \rho_f((\boldsymbol{u}_f^{n+1} - \boldsymbol{u}_m^{n+1})\cdot\nabla)\boldsymbol{u}_f^{n+1} \\
\qquad -\nabla\cdot\boldsymbol{T}_f^{n+1}(\boldsymbol{u}_f^{n+1}, p_f^{n+1}) = \boldsymbol{f}_f^{n+1} + \rho_f \boldsymbol{f}_{f,W}^{n+1} & \text{in } \Omega_f^{n+1}, \\
\nabla\cdot\boldsymbol{u}_f^{n+1} = 0 & \text{in } \Omega_f^{n+1}, \\
\rho_s \dfrac{\xi_{s,0}}{\Delta t^2}\widetilde{\boldsymbol{\eta}}_s^{n+1} + \mathcal{D}\left(\dfrac{\beta_{s,0}}{\Delta t}\widetilde{\boldsymbol{\eta}}_s^{n+1}\right) - \nabla\cdot\widetilde{\boldsymbol{T}}_s^{n+1}(\widetilde{\boldsymbol{\eta}}_s^{n+1}) \\
\qquad = \widetilde{\boldsymbol{f}}_s^{n+1} + \mathcal{D}\left(\widetilde{\boldsymbol{f}}_{s,U}^{n+1}\right) + \rho_s\widetilde{\boldsymbol{f}}_{s,W}^{n+1} & \text{in } \Omega_s^0, \\
\boldsymbol{u}_f^{n+1} = \boldsymbol{u}_s^{n+1} & \text{on } \Sigma^{n+1}, \\
\boldsymbol{T}_s^{n+1}(\boldsymbol{\eta}_s^{n+1})\,\boldsymbol{n} - \boldsymbol{T}_f^{n+1}(\boldsymbol{u}_f^{n+1}, p_f^{n+1})\,\boldsymbol{n} = \boldsymbol{0} & \text{on } \Sigma^{n+1}, \\
\alpha_e\widetilde{\boldsymbol{\eta}}_s^{n+1} + \widetilde{\boldsymbol{T}}_s^{n+1}(\widetilde{\boldsymbol{\eta}}_s^{n+1})\,\widetilde{\boldsymbol{n}} = P_{ext}\widetilde{\boldsymbol{n}} & \text{on } \Sigma_{out}^0,
\end{cases}
\tag{3}
$$

where

	BDF	Newmark/theta-methods
$\boldsymbol{f}_{s,U}^{n+1} :=$	$\displaystyle\sum_{i=1}^{p} \frac{\beta_{s,i}}{\Delta t}\boldsymbol{\eta}_s^{n+1-i}$	$\dfrac{\beta_{s,1}}{\Delta t}\boldsymbol{\eta}_s^n + \chi_s\boldsymbol{u}_s^n + \Delta t\kappa_s\boldsymbol{w}_s^n,$
$\boldsymbol{f}_{s,W}^{n+1} :=$	$\displaystyle\sum_{i=1}^{p+1} \frac{\xi_{s,i}}{\Delta t^2}\boldsymbol{\eta}_s^{n+1-i}$	$\dfrac{\xi_{s,1}}{\Delta t^2}\boldsymbol{\eta}_s^n + \dfrac{\sigma_s}{\Delta t}\boldsymbol{u}_s^n + \zeta_s\boldsymbol{w}_s^n,$
$\boldsymbol{f}_{f,W}^{n+1} :=$	$\displaystyle\sum_{i=1}^{p} \frac{\beta_{f,i}}{\Delta t}\boldsymbol{u}_f^{n+1-i}$	$\dfrac{\beta_{f,1}}{\Delta t}\boldsymbol{u}_f^n + \chi_f\boldsymbol{w}_f^n,$

are the forcing terms coming from the time discretization. In problem (3) we have also introduced the structure velocity $\boldsymbol{u}_s^n := \frac{\beta_{s,0}}{\Delta t}\boldsymbol{\eta}_s^n - \boldsymbol{f}_{s,U}^n$,

the structure acceleration $\boldsymbol{w}_s^n := \frac{\xi_{s,0}}{\Delta t^2}\boldsymbol{\eta}_s^n - \boldsymbol{f}_{s,W}^n$, and the fluid acceleration $\boldsymbol{w}_f^n := \frac{\beta_{f,0}}{\Delta t}\boldsymbol{u}_f^n - \boldsymbol{f}_{f,W}^n$. In Section 4 we provide concrete values for different sets of these parameters.

2. *Geometry problem.* Given the (unknown) interface structure displacement $\widetilde{\boldsymbol{\eta}}_s^{n+1}|_{\Sigma^0}$, solve a harmonic extension problem

$$\begin{cases} -\triangle\widetilde{\boldsymbol{\eta}}_m^{n+1} = \boldsymbol{0} & \text{in } \Omega_f^0, \\ \widetilde{\boldsymbol{\eta}}_m^{n+1} = \widetilde{\boldsymbol{\eta}}_s^{n+1} & \text{on } \Sigma^0, \end{cases} \tag{4}$$

and then find accordingly the discrete fluid domain velocity

$$\widetilde{\boldsymbol{u}}_m^{n+1} := \frac{\beta_{s,0}}{\Delta t}\widetilde{\boldsymbol{\eta}}_m^{n+1} - \widetilde{\boldsymbol{f}}_{m,U}^{n+1}, \tag{5}$$

and the points $\boldsymbol{x}_f^{n+1}$ of the new fluid domain by $\boldsymbol{x}_f^{n+1} = \boldsymbol{x}_f^0 + \widetilde{\boldsymbol{\eta}}_m^{n+1}$. Here $\widetilde{\boldsymbol{f}}_{m,U}^{n+1}$, $\widetilde{\boldsymbol{w}}_m^{n+1}$ and $\widetilde{\boldsymbol{f}}_{m,W}^{n+1}$ (the last two quantities are needed for the computation of $\widetilde{\boldsymbol{f}}_{m,U}^{n+1}$) are obtained using the same formulae as for $\boldsymbol{f}_{s,U}$, $\boldsymbol{w}_s$ and $\boldsymbol{f}_{s,W}$. Observe that $(4)_2$ guarantees that the displacement of the fluid interface coincides with that of the structure (geometrical conformity), whereas (5) guarantees that also the mesh and structure velocities coincide at the FS interface. The parameters introduced in the definitions of the forcing terms, of the structure velocity and of the accelerations, define completely the schemes, which are of order $q = p$ both for the fluid and for the structure subproblems for BDF schemes. The Newmark/theta-method schemes (for which $p = 1$) are in general of order $q = 1$, they becomes of order $q = 2$ for example for the particular choice *Midpoint/Crank-Nicolson*, which is the one considered in this work (see Section 4.2). The overall order of the FSI problem is then expected to be q, although no proofs are available so far in the literature, at the best of our knowledges.

2.3 A Lagrange multipliers-based formulation

In order to introduce suitable algorithms for the numerical solution of (3) and (4), we consider here an equivalent formulation based on the introduction of three Lagrange multipliers living at the FS interface, representing the fluid and structure normal stresses $\boldsymbol{\lambda}_f$ and $\boldsymbol{\lambda}_s$, and the normal derivative of the fluid mesh displacement $\boldsymbol{\lambda}_m$ (see the end of this section). These new unknowns are introduced just to simplify the expression of the three interface continuity conditions $(3)_{4-5}$ and $(4)_2$, and the derivation of the partitioned algorithms. However, we have not introduced them in our practical implementation of the algorithms to avoid extra costs.

We start by introducing some new notations. For the sake of notation we remove the temporal index $^{n+1}$. Given a space W, we denote with W^* its dual, with Σ_f^D and Σ_m^D we denote the parts of the boundary $\partial\Omega_f \setminus \Sigma$ where Dirichlet boundary conditions are prescribed for the fluid subproblem and for

the harmonic extension problem, respectively, and with $\Sigma_s^{D,0}$ the part of $\partial\Omega_s^0 \setminus \Sigma^0$ where Dirichlet conditions are prescribed for the structure subproblem. Then, we define the following spaces

$$V_f := \{v \in H^1(\Omega_f) : v|_{\Sigma_f^D} = 0\}, \qquad Q := L^2(\Omega_f)^1,$$

$$V_s := \{v \in H^1(\Omega_s^0) : v|_{\Sigma_s^{D,0}} = 0\}, \qquad V_m := \{v \in H^1(\Omega_f^0) : v|_{\Sigma_m^{D,0}} = 0\}.$$

Let $\mathcal{F} : [V_f]^3 \times Q \times [V_m]^3 \to ([V_f]^3 \times Q)^*$ be the fluid operator, defined by

$$< \mathcal{F}(\boldsymbol{u}_f, p, \boldsymbol{u}_m), (\boldsymbol{v}, q) >:=$$

$$\int_{\Omega_f} \left[\left(\rho_f \frac{\beta_{f,0}}{\Delta t} \boldsymbol{u}_f + \rho_f((\boldsymbol{u}_f - \boldsymbol{u}_m) \cdot \nabla)\boldsymbol{u}_f \right) \cdot \boldsymbol{v} + \boldsymbol{T}_f(\boldsymbol{u}_f, p_f) : \nabla \boldsymbol{v} - \nabla \cdot \boldsymbol{u}_f \, q \right] d\boldsymbol{x},$$

with $(\boldsymbol{v}, q) \in [V_f]^3 \times Q$, and let $\mathcal{G}_f$ be the operator related to the right hand side of the fluid momentum equation, that is

$$< \mathcal{G}_f, \boldsymbol{v} >:= \int_{\Omega_f} \left(\boldsymbol{f}_f^{n+1} + \rho_f \boldsymbol{f}_{f,W}^{n+1} \right) \cdot \boldsymbol{v} \, d\boldsymbol{x}.$$

Analogously, for the structure subproblem we define the operator $\mathcal{S} : [V_s]^3 \to ([V_s]^3)^*$ as follows

$$< \mathcal{S}(\widetilde{\boldsymbol{\eta}}_s), \widetilde{\boldsymbol{\mu}} >:= \int_{\Omega_s^0} \left[\left(\rho_s \frac{\xi_{s,0}}{\Delta t^2} \widetilde{\boldsymbol{\eta}}_s + \mathcal{D}\left(\frac{\beta_{s,0}}{\Delta t} \widetilde{\boldsymbol{\eta}}_s \right) \right) \cdot \widetilde{\boldsymbol{\mu}} + \widetilde{\boldsymbol{T}}_s(\widetilde{\boldsymbol{\eta}}_m) : \nabla \widetilde{\boldsymbol{\mu}} \right] d\boldsymbol{x}^0,$$

with $\widetilde{\boldsymbol{\mu}} \in [V_s]^3$, and $\mathcal{G}_s$ as follows

$$< \mathcal{G}_s, \widetilde{\boldsymbol{\mu}} >:= \int_{\Omega_s^0} \left(\widetilde{\boldsymbol{f}}_s^{n+1} + \mathcal{D}(\widetilde{\boldsymbol{f}}_{s,U}^{n+1}) + \rho_s \widetilde{\boldsymbol{f}}_{s,W}^{n+1} \right) \cdot \widetilde{\boldsymbol{\mu}} \, d\boldsymbol{x}^0,$$

with $\widetilde{\boldsymbol{\mu}} \in [V_s]^3$. Finally, for the harmonic extension, we introduce the operator $\mathcal{H} : [V_m]^3 \to ([V_m]^3)^*$ defined as

$$< \mathcal{H}(\widetilde{\boldsymbol{\eta}}_m), \widetilde{\boldsymbol{z}} >:= \int_{\Omega_f^0} \nabla \widetilde{\boldsymbol{\eta}}_m : \nabla \widetilde{\boldsymbol{z}} \, d\boldsymbol{x}^0,$$

with $\widetilde{\boldsymbol{z}} \in [V_m]^3$. We also define the following trace operators

$$\begin{array}{l} \widetilde{\gamma}_f : [V_f]^3 \to [H^{1/2}(\Sigma^0)]^3, \ \widetilde{\gamma}_f \boldsymbol{v} := \widetilde{\boldsymbol{v}}|_{\Sigma^0}, \\ \widetilde{\gamma}_s : [V_s]^3 \to [H^{1/2}(\Sigma^0)]^3, \ \widetilde{\gamma}_s \widetilde{\boldsymbol{\mu}} := \widetilde{\boldsymbol{\mu}}|_{\Sigma^0}, \\ \widetilde{\gamma}_m : [V_m]^3 \to [H^{1/2}(\Sigma^0)]^3, \ \widetilde{\gamma}_m \widetilde{\boldsymbol{z}} := \widetilde{\boldsymbol{z}}|_{\Sigma^0}, \end{array} \tag{6}$$

[1]Since we solve the FSI problem in a partitioned way with Robin conditions at the FS interface (see (9)), the pressure is always defined and $L^2(\Omega_f)$ is the suitable pressure space for the weak formulation.

and the related adjoint operators as follows

$$\begin{array}{l}\widetilde{\gamma}_f^* : [H^{-1/2}(\Sigma^0)]^3 \to ([V_f]^3)^*, < \widetilde{\gamma}_f^* \widetilde{\boldsymbol{\lambda}}, \boldsymbol{v} >:=< \widetilde{\boldsymbol{\lambda}}, \widetilde{\gamma}_f \boldsymbol{v} > \ \forall \boldsymbol{v} \in [V_f]^3, \\ \widetilde{\gamma}_s^* : [H^{-1/2}(\Sigma^0)]^3 \to ([V_s]^3)^*, < \widetilde{\gamma}_s^* \widetilde{\boldsymbol{\lambda}}, \widetilde{\boldsymbol{\mu}} >:=< \widetilde{\boldsymbol{\lambda}}, \widetilde{\gamma}_s \widetilde{\boldsymbol{\mu}} > \ \forall \widetilde{\boldsymbol{\mu}} \in [V_s]^3, \\ \widetilde{\gamma}_m^* : [H^{-1/2}(\Sigma^0)]^3 \to ([V_m]^3)^*, < \widetilde{\gamma}_m^* \widetilde{\boldsymbol{\lambda}}, \widetilde{\boldsymbol{z}} >:=< \widetilde{\boldsymbol{\lambda}}, \widetilde{\gamma}_m \widetilde{\boldsymbol{z}} > \ \forall \widetilde{\boldsymbol{z}} \in [V_m]^3. \end{array} \tag{7}$$

For functions regular enough, from previous definitions we have

$$\begin{array}{rcl} < \widetilde{\gamma}_f^* \widetilde{\boldsymbol{\lambda}}, \boldsymbol{v} > & = & \displaystyle\int_{\Sigma^0} \widetilde{\boldsymbol{\lambda}} \cdot \widetilde{\boldsymbol{v}} \, d\sigma^0, \\ < \widetilde{\gamma}_s^* \widetilde{\boldsymbol{\lambda}}, \widetilde{\boldsymbol{\mu}} > & = & \displaystyle\int_{\Sigma^0} \widetilde{\boldsymbol{\lambda}} \cdot \widetilde{\boldsymbol{\mu}} \, d\sigma^0, \\ < \widetilde{\gamma}_m^* \widetilde{\boldsymbol{\lambda}}, \widetilde{\boldsymbol{z}} > & = & \displaystyle\int_{\Sigma^0} \widetilde{\boldsymbol{\lambda}} \cdot \widetilde{\boldsymbol{z}} \, d\sigma^0. \end{array} \tag{8}$$

We observe that the trace operator for fluid quantities returns the trace in the *reference configuration*.

We are now ready to rewrite problem (3)-(4) as follows

$$\left\{ \begin{array}{rcll} \mathcal{H}(\widetilde{\boldsymbol{\eta}}_m) + \widetilde{\gamma}_m^* \widetilde{\boldsymbol{\lambda}}_m & = & \boldsymbol{0} & \text{in } ([V_m]^3)^*, \\ \widetilde{\gamma}_m \widetilde{\boldsymbol{\eta}}_m & = & \widetilde{\gamma}_s \widetilde{\boldsymbol{\eta}}_s & \text{on } \Sigma^0, \\ \mathcal{F}(\boldsymbol{u}_f, p_f, \boldsymbol{u}_m) + \widetilde{\gamma}_f^* \widetilde{\boldsymbol{\lambda}}_f & = & \mathcal{G}_f & \text{in } ([V_f]^3)^*, \\ \alpha_f \, \widetilde{\gamma}_f \boldsymbol{u}_f + \widetilde{\boldsymbol{\lambda}}_f & = & \alpha_f \left(\frac{\beta_{s,0}}{\Delta t} \widetilde{\gamma}_s \widetilde{\boldsymbol{\eta}}_s - \widetilde{\boldsymbol{f}}_{s,U} \right) - \widetilde{\boldsymbol{\lambda}}_s & \text{on } \Sigma^0, \\ \alpha_s \frac{\beta_{s,0}}{\Delta t} \, \widetilde{\gamma}_s \widetilde{\boldsymbol{\eta}}_s + \widetilde{\boldsymbol{\lambda}}_s & = & \alpha_s \widetilde{\gamma}_f \boldsymbol{u}_f - \widetilde{\boldsymbol{\lambda}}_f + \alpha_s \widetilde{\gamma}_s \widetilde{\boldsymbol{f}}_{s,U} & \text{on } \Sigma^0, \\ \mathcal{S}(\widetilde{\boldsymbol{\eta}}_s) + \widetilde{\gamma}_s^* \widetilde{\boldsymbol{\lambda}}_s & = & \mathcal{G}_s & \text{in } ([V_s]^3)^*, \end{array} \right. \tag{9}$$

where the interface continuity conditions $(9)_{4-5}$ are linear combinations of conditions $(3)_{4-5}$, through the introduction of two functions in $L^\infty(\Sigma^0)$, $\alpha_f \neq \alpha_s$. This will be useful to derive partitioned procedures based on Robin interface conditions (Robin-Robin (RR) schemes, see [5, 25, 26, 27]). This approach has good convergence properties, independent of the added-mass effect (which is very high in haemodynamic contexts, see [15]) when the parameters α_f and α_s are suitably chosen, as shown in [5, 27]. Moreover, we point out that these conditions together with $(9)_2$ are written in the *reference configuration*. This choice will simplify the computation of the derivative in the Newton method, as it will be clear in the next section.

We give now a characterization of the Lagrange multipliers introduced. From the definition of $\mathcal{F}$, by taking $\boldsymbol{v}$ as a divergence free extension of a function $\boldsymbol{\phi} \in [H^{1/2}(\Sigma)]^3$, zero on Σ_f^D, and integrating by parts, we have

$$\begin{aligned} 0 &=< -\mathcal{G}_f + \mathcal{F}(\boldsymbol{u}_f, p_f, \boldsymbol{u}_m), (\boldsymbol{v}, 0) > + < \widetilde{\gamma}_f^* \widetilde{\boldsymbol{\lambda}}_f, \boldsymbol{v} > \\ &= - \int_\Sigma \boldsymbol{T}_f(\boldsymbol{u}_f, p_f) \, \boldsymbol{n} \cdot \boldsymbol{\phi} \, d\sigma + < \widetilde{\boldsymbol{\lambda}}_f, \widetilde{\gamma}_f \boldsymbol{v} > . \end{aligned}$$

If $\boldsymbol{\lambda}_f$ is regular enough, we obtain thanks to (8)

$$-\int_\Sigma \boldsymbol{T}_f(\boldsymbol{u}_f,p_f)\,\boldsymbol{n}\cdot\boldsymbol{\phi}\,d\sigma+<\widetilde{\boldsymbol{\lambda}}_f,\widetilde{\gamma}_f\boldsymbol{v}>=-\int_\Sigma \boldsymbol{T}_f(\boldsymbol{u}_f,p_f)\,\boldsymbol{n}\cdot\boldsymbol{\phi}\,d\sigma+\int_{\Sigma^0}\widetilde{\boldsymbol{\lambda}}_f\cdot\widetilde{\boldsymbol{\phi}}\,d\sigma^0=0.$$

We introduce now the quantities $\boldsymbol{F}_{ALE}:=\nabla_{\boldsymbol{x}_f^0}\boldsymbol{x}_f$, and $J_{ALE}:=det(\boldsymbol{F}_{ALE})$. Then, from the Nanson formula $\boldsymbol{n}\,d\sigma=J_{ALE}\boldsymbol{F}_{ALE}^{-T}\widetilde{\boldsymbol{n}}\,d\sigma^0$, we obtain

$$-\int_{\Sigma^0} J_{ALE}\boldsymbol{T}_f(\boldsymbol{u}_f,p_f)\boldsymbol{F}_{ALE}^{-T}\widetilde{\boldsymbol{n}}\cdot\widetilde{\boldsymbol{\phi}}\,d\sigma^0+\int_{\Sigma^0}\widetilde{\boldsymbol{\lambda}}_f\cdot\widetilde{\boldsymbol{\phi}}\,d\sigma^0=0.$$

Since the previous identity holds for all $\boldsymbol{\phi}\in[H^{1/2}(\Sigma)]^3$, we obtain

$$\widetilde{\boldsymbol{\lambda}}_f=\left(J_{ALE}\,\boldsymbol{T}_f(\boldsymbol{u}_f,p_f)\boldsymbol{F}_{ALE}^{-T}\widetilde{\boldsymbol{n}}\right)\Big|_{\Sigma^0}=\left(\widetilde{\boldsymbol{T}}_f(\widetilde{\boldsymbol{u}}_f,\widetilde{p}_f)\widetilde{\boldsymbol{n}}\right)\Big|_{\Sigma^0},$$

which shows that the Lagrange multiplier $\boldsymbol{\lambda}_f$ has the physical meaning of the fluid normal stress at the FS interface *in the reference configuration*. With analogous steps, we obtain

$$\widetilde{\boldsymbol{\lambda}}_s=-\left(\widetilde{\boldsymbol{T}}_s(\widetilde{\boldsymbol{\eta}}_s)\widetilde{\boldsymbol{n}}\right)\Big|_{\Sigma^0},\qquad \widetilde{\boldsymbol{\lambda}}_m=\frac{\partial\widetilde{\boldsymbol{\eta}}_m}{\partial\widetilde{\boldsymbol{n}}}\Big|_{\Sigma^0}.$$

3 Numerical algorithms

For the solution of the FSI problem (9), we propose to use a general preconditioned Richardson method

$$\widehat{F}(y^k)\,\delta y^{k+1}=-F(y^k),\tag{10}$$

where y^k denotes the FSI solution $[\widetilde{\boldsymbol{\eta}}_m^k,\widetilde{\boldsymbol{\lambda}}_m^k,\boldsymbol{v}_f^k,\widetilde{\boldsymbol{\lambda}}_f^k,\widetilde{\boldsymbol{\lambda}}_s^k,\widetilde{\boldsymbol{\eta}}_s^k]$ at the generic subiteration k, with $\boldsymbol{v}_f:=(\boldsymbol{u}_f,p_f)$, δy^{k+1} is the increment of the FSI solution at the new iteration $k+1$ with respect to y^k, $F(y)=0$ corresponds to problem (9), and $\widehat{F}$ is a suitable preconditioner.

We mainly distiguish two families of preconditioners, those derived from the Newton method and those derived from quasi-Newton methods. In particular, the Newton method is given by (10) with

$$\widehat{F}=\nabla F=\left[\begin{array}{cc|cc|cc}
\mathcal{H} & \widetilde{\gamma}_m^* & & & & \\
\widetilde{\gamma}_m & & & & & -\widetilde{\gamma}_s \\
\hline
\nabla_{u_m}\mathcal{F} & & \nabla_{v_f}\mathcal{F} & \widetilde{\gamma}_f^* & & \\
 & & \alpha_f\widetilde{\gamma}_f & I & I & -\alpha_f\frac{\beta_{s,0}}{\Delta t}\widetilde{\gamma}_s \\
\hline
 & & -\alpha_s\widetilde{\gamma}_f & I & I & \alpha_s\frac{\beta_{s,0}}{\Delta t}\widetilde{\gamma}_s \\
 & & & & \widetilde{\gamma}_s^* & \nabla_{\eta_s}\mathcal{S}
\end{array}\right].$$

This is obtained by taking only *material derivatives*, i.e. the differentiation is done with respect to the unknowns in the *reference configuration*. By doing this,

the trace operators introduced in (6) and (7) are *linear* and the differentiation of the interface conditions becomes trivial. We point out however that the operator $\mathcal{F}$ heavily depends on the unknown ALE mapping $\boldsymbol{\eta}_m$ and this introduces *shape derivatives* in the term $\nabla_{u_m}\mathcal{F}$.

Another class of schemes is given by quasi-Newton methods. In this case, we consider the approximation

$$\widehat{F} = \widehat{J} = \left[\begin{array}{cc|ccc} \mathcal{H} & \widetilde{\gamma}_m^* & & & \\ \widetilde{\gamma}_m & & & & -\widetilde{\gamma}_s \\ \hline & & \widehat{\nabla}_{v_f}\mathcal{F} & \widetilde{\gamma}_f^* & \\ & & \alpha_f\widetilde{\gamma}_f & I & I \quad -\alpha_f\frac{\beta_{s,0}}{\Delta t}\widetilde{\gamma}_s \\ \hline & & -\alpha_s\widetilde{\gamma}_f & I & I \quad \alpha_s\frac{\beta_{s,0}}{\Delta t}\widetilde{\gamma}_s \\ & & & & \widetilde{\gamma}_s^* \quad \nabla_{\eta_s}\mathcal{S} \end{array}\right],$$

where $\widehat{\nabla}_{v_f}\mathcal{F}\,\delta\boldsymbol{v}_f := \left\{\begin{array}{l} \rho_f\dfrac{\beta_{f,0}}{\Delta t}\delta\boldsymbol{u}_f + \rho_f((\boldsymbol{u}_f-\boldsymbol{u}_m)\cdot\nabla)\delta\boldsymbol{u}_f - \nabla\cdot\boldsymbol{T}_f(\delta\boldsymbol{u}_f,\delta p_f) \\ \nabla\cdot\delta\boldsymbol{u}_f \end{array}\right.$,

that is we have skipped the term $(\delta\boldsymbol{u}_f\cdot\nabla)\boldsymbol{u}_f$. Moreover, we do not consider the shape derivatives $\nabla_{u_m}\mathcal{F}$. This leads to the Oseen approximation of the Navier-Stokes problem obtained by using as convective term previous solutions $\boldsymbol{u}_f$ and $\boldsymbol{u}_m$.

We are ready now to derive from ∇F and $\widehat{J}$ other preconditioners $\widehat{F}$, leading to suitable algorithms for the numerical solution of (9). We detail them for the case of the quasi-Newton approximation, deriving them by approximating $\widehat{J}$, being their extension to the Newton case straightforward. In all cases, the stopping criterion is given by the computation of the residual $F(y)$, that is

$$\|F(y^{k+1})\|_Y \le \varepsilon_1 + \varepsilon_2\|y_R^{k+1}\|_Y,$$

where Y is the global space where the solution y belongs to and ε_1 and ε_2 are given tolerances. We observe that in the previous definition we use both an absolute and a relative criterion, so that we say that convergence is achieved when both criteria are satisfied. In particular, the normalization is done with respect to the term y_R, which is properly chosen case by case. By considering (10), an equivalent stopping criterion (more useful from the practical point of view) is

$$\|F(y^{k+1}) - \widehat{F}(y^k)\delta y^{k+1} - F(y^k)\|_Y \le \varepsilon_1 + \varepsilon_2\|y_R^{k+1}\|_Y. \tag{11}$$

In what follows we consider a linear elastic vascular wall. This choice aims at focusing on the geometrical non-linearity only. The extension and validation of the proposed schemes to other, more complex, non-linear constitutive laws is under investigation. Therefore, in what follows, we have $\nabla_{\eta_s}\mathcal{S} \equiv \mathcal{S}$, and we write the following schemes in non-incremental form.

3.1 Single-loop algorithm

We consider the following *three block Gauss-Seidel* preconditioner (see also [12])

$$\widehat{J}_{SL} = \left[\begin{array}{cc|cc|cc} \mathcal{H} & \widetilde{\gamma}_m^* & & & & \\ \widetilde{\gamma}_m & & & & & \\ \hline & & \widehat{\nabla}_{v_f}\mathcal{F} & \widetilde{\gamma}_f^* & & \\ & & \alpha_f\widetilde{\gamma}_f & I & & \\ \hline & & -\alpha_s\widetilde{\gamma}_f & I & I & \alpha_s\frac{\beta_{s,0}}{\Delta t}\widetilde{\gamma}_s \\ & & & & \widetilde{\gamma}_s^* & \mathcal{S} \end{array}\right],$$

which corresponds to the sequential solution of the harmonic extension, fluid subproblem and structure subproblem, leading to the following algorithm:

Given the solution at iteration k, solve at the current iteration $k+1$ until convergence

1. The harmonic extension

$$\begin{cases} -\triangle\widetilde{\boldsymbol{\eta}}_m^{k+1} = \mathbf{0} & \text{in } \Omega_f^0, \\ \widetilde{\gamma}_m\,\widetilde{\boldsymbol{\eta}}_m^{k+1} = \widetilde{\gamma}_s\,\widetilde{\boldsymbol{\eta}}_s^{k} & \text{on } \Sigma^0, \end{cases}$$

   obtaining the new fluid domain Ω_f^{k+1} and the fluid domain velocity $\boldsymbol{u}_m^{k+1}$.

2. The fluid subproblem with a Robin condition at the FS interface

$$\begin{cases} \rho_f\dfrac{\beta_{f,0}}{\Delta t}\boldsymbol{u}_f^{k+1} + \rho_f((\boldsymbol{u}_f^k - \boldsymbol{u}_m^{k+1})\cdot\nabla)\boldsymbol{u}_f^{k+1} - \nabla\cdot\boldsymbol{T}_f(\boldsymbol{u}_f^{k+1}, p_f^{k+1}) = \boldsymbol{f}_f + \rho_f\boldsymbol{f}_{f,W} & \text{in } \Omega_f^{k+1}, \\ \nabla\cdot\boldsymbol{u}_f^{k+1} = 0 & \text{in } \Omega_f^{k+1}, \\ \alpha_f\,\gamma_f\,\boldsymbol{u}_f^{k+1} + \boldsymbol{T}_f(\boldsymbol{u}_f^{k+1}, p_f^{k+1}) = \alpha_f\left(\dfrac{\beta_{s,0}}{\Delta t}\gamma_s\boldsymbol{\eta}_s^k - \boldsymbol{f}_{s,U}\right) + \boldsymbol{T}_s(\boldsymbol{\eta}^k) & \text{on } \Sigma^{k+1}; \end{cases}$$

3. The structure subproblem with a Robin condition at the FS interface

$$\begin{cases} \rho_s\dfrac{\xi_{s,0}}{\Delta t^2}\widetilde{\boldsymbol{\eta}}_s^{k+1} + \mathcal{D}\left(\dfrac{\beta_{s,0}}{\Delta t}\widetilde{\boldsymbol{\eta}}_s^{k+1}\right) - \nabla\cdot\widetilde{\boldsymbol{T}}_s(\widetilde{\boldsymbol{\eta}}_s^{k+1}) = \widetilde{\boldsymbol{f}}_s + \mathcal{D}(\widetilde{\boldsymbol{f}}_{s,U}) + \rho_s\widetilde{\boldsymbol{f}}_{s,W} & \text{in } \Omega_s^0, \\ \alpha_s\dfrac{\beta_{s,0}}{\Delta t}\,\widetilde{\gamma}_s\,\widetilde{\boldsymbol{\eta}}_s^{k+1} - \widetilde{\boldsymbol{T}}_s(\widetilde{\boldsymbol{\eta}}_s^{k+1}) = \alpha_s\widetilde{\gamma}_f\,\widetilde{\boldsymbol{u}}_f^{k+1} - \widetilde{\boldsymbol{T}}_f(\widetilde{\boldsymbol{u}}_f^{k+1}, \widetilde{p}_f^{k+1})\widetilde{\boldsymbol{n}} + \alpha_s\widetilde{\boldsymbol{f}}_{s,U} & \text{on } \Sigma^0. \end{cases}$$

Here $\gamma_i : [V_i]^3 \to H^{1/2}(\Sigma)$, $i = f, s$ are the trace operators defined as $\gamma_i\boldsymbol{v} := \boldsymbol{v}|_\Sigma$, $\boldsymbol{v} \in [V_i]^3$, $i = f, s$, on the deformed interface.

From (11), we obtain the following stopping criterion

$$\|\widetilde{\gamma}_s\,\widetilde{\boldsymbol{\eta}}_s^{k+1} - \widetilde{\gamma}_s\,\widetilde{\boldsymbol{\eta}}_s^{k}\|_X + \|((\boldsymbol{u}_f^{k+1} - \boldsymbol{u}_f^k)\cdot\nabla)\,\boldsymbol{u}_f^{k+1}\|_W \tag{12}$$

$$+ \left\|\frac{\alpha_f\beta_{s,0}}{\Delta t}\left(\widetilde{\gamma}_s\widetilde{\boldsymbol{\eta}}_s^{k+1} - \widetilde{\gamma}_s\widetilde{\boldsymbol{\eta}}_s^{k}\right) + \widetilde{\boldsymbol{\lambda}}_s^{k+1} - \widetilde{\boldsymbol{\lambda}}_s^{k}\right\|_Z$$

$$\leq \varepsilon_1 + \varepsilon_2 \min\left\{ \|\widetilde{\boldsymbol{\eta}}_s^{k+1}\|_X; \|(\boldsymbol{u}_f^{k+1}\cdot\nabla)\boldsymbol{u}_f^{k+1}\|_W; \left\| \frac{\alpha_f\beta_{s,0}}{\Delta t}\widetilde{\gamma}_s\widetilde{\boldsymbol{\eta}}_s^{k+1} + \widetilde{\boldsymbol{\lambda}}_s^{k+1} \right\|_Z \right\}.$$

Here X, W, Z are suitable Sobolev spaces. In particular, the right choice would be $X = H^{1/2}(\Sigma^0)$, $W = H^{-1}(\Omega_f)$, $Z = H^{-1/2}(\Sigma^0)$. However, due to the complexity in the computation of the latter two norms, in pratical implementations we consider $W = L^2(\Omega_f)$ and $Z = L^2(\Sigma^0)$.

This scheme is the most classical for haemodynamics applications (see, e.g., [20]), although we present it here with Robin-Robin interface conditions instead of the more common Dirichlet-Neumann choice. However, the use of just one loop for the treatment of both geometrical/physical non-linearities and interface continuity conditions, does not gurantee *a priori* a fast convergence towards the exact solution.

3.2 Double-loop algorithm

We consider the following *two block Gauss-Seidel* preconditioner

$$\widehat{J}_{DL} = \left[\begin{array}{cc|cc|cc} \mathcal{H} & \widetilde{\gamma}_m^* & & & & \\ \widetilde{\gamma}_m & & & & & \\ \hline & & \widehat{\nabla}_{v_f}\mathcal{F} & \widetilde{\gamma}_f^* & & \\ & & \alpha_f\widetilde{\gamma}_f & I & I & -\alpha_f\frac{\beta_{s,0}}{\Delta t}\widetilde{\gamma}_s \\ \hline & & -\alpha_s\widetilde{\gamma}_f & I & I & \alpha_s\frac{\beta_{s,0}}{\Delta t}\widetilde{\gamma}_s \\ & & & & \widetilde{\gamma}_s^* & \mathcal{S} \end{array}\right],$$

which corresponds to the sequential solution of the harmonic extension and of a linearized FSI problem. For the solution of the latter, since we are interested in partitioned algorithms, we use the following preconditioner (see [5])

$$\widehat{P}_{RR} = \left[\begin{array}{cc|cc} \widehat{\nabla}_{v_f}\mathcal{F} & \widetilde{\gamma}_f^* & & \\ \alpha_f\widetilde{\gamma}_f & I & & \\ \hline -\alpha_s\widetilde{\gamma}_f & I & I & \alpha_s\frac{\beta_{s,0}}{\Delta t}\widetilde{\gamma}_s \\ & & \widetilde{\gamma}_s^* & \mathcal{S} \end{array}\right].$$

This corresponds to consider two nested loops, an external one for the treatment of the interface position through a fixed-point (quasi-Newton) scheme, and an internal one for the treatment of the interface continuity conditions through the RR scheme. In particular, we have the following algorithm:

Given the solution at iteration k, solve at the current iteration $k+1$ until convergence (we omit the superscript $^{k+1}$)

1. The harmonic extension

$$\begin{cases} -\triangle\widetilde{\boldsymbol{\eta}}_m = \mathbf{0} & \text{in } \Omega_f^0, \\ \widetilde{\gamma}_m\,\widetilde{\boldsymbol{\eta}}_m = \widetilde{\gamma}_s\,\widetilde{\boldsymbol{\eta}}_s^k & \text{on } \Sigma^0, \end{cases}$$

obtaining the new fluid domain Ω_f and the fluid domain velocity $\boldsymbol{u}_m$.

2. The linearized FSI problem. In particular, given the solution at subiteration $l-1$, solve at the current subiteration l until convergence

   (a) The fluid subproblem with a Robin condition at the FS interface

$$\begin{cases} \rho_f \dfrac{\beta_{f,0}}{\Delta t}\boldsymbol{u}_{f,l} + \rho_f((\boldsymbol{u}_f^k - \boldsymbol{u}_m)\cdot\nabla)\boldsymbol{u}_{f,l} - \nabla\cdot\boldsymbol{T}_f(\boldsymbol{u}_{f,l},p_{f,l}) = \boldsymbol{f}_f + \rho_f\boldsymbol{f}_{f,W} & \text{in } \Omega_f, \\ \nabla\cdot\boldsymbol{u}_{f,l} = 0 & \text{in } \Omega_f, \\ \alpha_f\,\gamma_f\,\boldsymbol{u}_{f,l} + \boldsymbol{T}_f(\boldsymbol{u}_{f,l},p_{f,l}) = \alpha_f\left(\dfrac{\beta_{s,0}}{\Delta t}\gamma_s\boldsymbol{\eta}_{s,l-1} - \boldsymbol{f}_{s,U}\right) + \boldsymbol{T}_s(\boldsymbol{\eta}_{l-1}) & \text{on } \Sigma; \end{cases}$$

   (b) The structure subproblem with a Robin condition at the FS interface

$$\begin{cases} \rho_s\dfrac{\xi_{s,0}}{\Delta t^2}\widetilde{\boldsymbol{\eta}}_{s,l} + \mathcal{D}\left(\dfrac{\beta_{s,0}}{\Delta t}\widetilde{\boldsymbol{\eta}}_{s,l}\right) - \nabla\cdot\boldsymbol{T}_s(\widetilde{\boldsymbol{\eta}}_{s,l}) = \widetilde{\boldsymbol{f}}_s + \mathcal{D}(\widetilde{\boldsymbol{f}}_{s,U}) + \rho_s\widetilde{\boldsymbol{f}}_{s,W} & \text{in } \Omega_s^0, \\ \alpha_s\dfrac{\beta_{s,0}}{\Delta t}\,\widetilde{\gamma}_s\,\widetilde{\boldsymbol{\eta}}_{s,l} - \widetilde{\boldsymbol{T}}_s(\widetilde{\boldsymbol{\eta}}_{s,l}) = \alpha_s\widetilde{\gamma}_f\,\widetilde{\boldsymbol{u}}_{f,l} - \widetilde{\boldsymbol{T}}_f(\widetilde{\boldsymbol{u}}_{f,l},\widetilde{p}_{f,l})\widetilde{\boldsymbol{n}} + \alpha_s\widetilde{\boldsymbol{f}}_{s,U} & \text{on } \Sigma^0. \end{cases}$$

From (11), we obtain the following stopping criterion for the external loop

$$\begin{aligned} &\|\widetilde{\gamma}_s\,\widetilde{\boldsymbol{\eta}}_s - \widetilde{\gamma}_s\,\widetilde{\boldsymbol{\eta}}_s^k\|_X + \|((\boldsymbol{u}_f - \boldsymbol{u}_f^k)\cdot\nabla)\,\boldsymbol{u}_f\|_W \\ &\leq \varepsilon_1 + \varepsilon_2\min\left\{\|\widetilde{\boldsymbol{\eta}}_s\|_X; \|(\boldsymbol{u}_f\cdot\nabla)\boldsymbol{u}_f\|_W\right\}, \end{aligned} \tag{13}$$

while for the internal loop we have (see [5])

$$\left\|\frac{\alpha_f\beta_{s,0}}{\Delta t}\left(\widetilde{\gamma}_s\widetilde{\boldsymbol{\eta}}_{s,l} - \widetilde{\gamma}_s\,\widetilde{\boldsymbol{\eta}}_{s,l-1}\right) + \widetilde{\boldsymbol{\lambda}}_{s,l} - \widetilde{\boldsymbol{\lambda}}_{s,l-1}\right\|_Z \leq \varepsilon_3 + \varepsilon_4\left\|\frac{\alpha_f\beta_{s,0}}{\Delta t}\widetilde{\gamma}_s\widetilde{\boldsymbol{\eta}}_{s,l} + \widetilde{\boldsymbol{\lambda}}_{s,l}\right\|_Z. \tag{14}$$

The use of two different loops for the geometrical/physical non-linearities and for the imposition of the interface continuity conditions makes this scheme more robust with respect to *Single-loop*.

3.3 Inexact solutions

In order to improve the performances of the proposed algorithms in terms of CPU time, we propose here two families of algorithms drawn from the *Double-loop* scheme. In particular, we consider the *geometrical and convective inexact schemes-m* (GCIS-m), obtained from Double-loop by performing at most m iterations in the external loop, and the *interface conditions inexact scheme-n* (ICIS-n), obtained by performing at most n RR iterations in the internal loop. We observe that with GCIS-1 we perform just one external iteration, that is we solve a linearized FSI problem in a known domain (see [9, 10, 11, 12]).

For what concernes the stopping criterion, one has to consider (13) for ICIS-n schemes, while (14) for GCIS-m schemes.

3.4 Extrapolation from previous time steps

We are also interested in studying how the accuracy and/or the number of (external) iterations of the proposed schemes could be possibly improved when considering at each new time step suitable extrapolations of order q of the interface quantities and fluid convective term, from previous time steps, q being the the order of the temporal schemes. To this aim, we refer to the schemes with extrapolation as *Double-loop-extrap*, *Single-loop-extrap* and *GCIS-m-extrap*. We anticipate here that no improvemens are noticed in the numerical experiments by using GCIS-m-extrap with respect to GCIS-m, with $m \geq 2$. For this reason, among the GCIS-m-extrap schemes we consider just GCIS-1-extrap. In particular, this scheme is obtained by performing just one external iteration as for GCIS-1, but using as fluid domain quantities and convective term, extrapolations of order q from previous time steps. Obviously, GCIS-1 and GCIS-1-extrap do coincide for first order approximations.

In any case, for BDF schemes the extrapolation of order q of the FS interface and of the convective term is obtained by setting at the first external iteration $k = 0$

$$\boldsymbol{z}^{n+1,0} = \sum_{i=0}^{p} i\beta_i \boldsymbol{z}^{n+1-i},$$

where $\boldsymbol{z}$ is one of the exrapolated variables, namely the fluid velocity, the fluid mesh velocity and the interface structure displacement. For the Newmark scheme, since it is at most second order accurate, we use the following extrapolation

$$\boldsymbol{z}^{n+1,0} = \boldsymbol{z}^{n} + \Delta t \boldsymbol{d}^{n},$$

where $\boldsymbol{d}$ is the discrete approximation of the time derivative of $\boldsymbol{z}$.

4 Numerical results

4.1 Generalities

In all the numerical simulations considered in this work, we assume that the solid is a linear elastic material, characterized by the following Piola-Kirchhoff stress tensor

$$\widetilde{\boldsymbol{T}}_s = \frac{E}{2(1+\nu)}\boldsymbol{\epsilon}(\widetilde{\boldsymbol{\eta}}_s) + \frac{E\nu}{(1+\nu)(1-2\nu)}\,\mathrm{tr}(\boldsymbol{\epsilon}(\widetilde{\boldsymbol{\eta}}_s))\,\boldsymbol{I}, \tag{15}$$

where $\boldsymbol{\epsilon}(\boldsymbol{\eta}) := \frac{(\nabla\boldsymbol{\eta}+(\nabla\boldsymbol{\eta})^T)}{2}$, E is the Young modulus, and ν is the Poisson ratio. We also consider the FSI problem (1), with $\mathcal{D} = 0$. Moreover, if not otherwise specified, we use $P1bubble - P1$ finite elements for the fluid subproblem and $P1$ finite elements for the structure subproblem, and the following data: viscosity $\mu = 0.03\,dyne/cm^2$, fluid density $\rho_f = 1\,g/cm^3$, structure density $\rho_s = 1.2\,g/cm^3$, Young modulus $E = 3 \cdot 10^6\,dyne/cm^2$, Poisson ratio $\nu = 0.45$,

time discretization parameter $\Delta t = 0.001\, s$, and elastic coefficient of the surrounding tissue $\alpha_e = 3 \cdot 10^6\, dyne/cm^2$. This value has been extracted by the experimental results reported in [22] and allows to recover a pressure in the physiological range.

For the prescription of the interface continuity conditions, in all the simulations we have considered the RR scheme, with the optimal coefficients proposed in [27]. In particular, the optimization procedure adapted to the various temporal schemes leads to

$$\alpha_f = \frac{1}{\beta_{s,0}} \left(\frac{\xi_{s,0} \rho_s H_s}{\Delta t} + \tau \Delta t \right),$$

where $\tau := \frac{E H_s \sqrt{\pi}}{(1-\nu^2) R^2}$, with R a reference radius, and

$$\alpha_s = \frac{2}{\Delta t\, k^*} \sqrt{\rho_f + \mu \Delta t\, (k^*)^2} \left(\sqrt{\mu \Delta t}\, k^* + \sqrt{\rho_f + \mu \Delta t\, (k^*)^2} \right),$$

with $k^* = \sqrt{\frac{\beta_{f,0} \rho_f (\sqrt{5}-1)}{2 \mu \Delta t}}$. In all the simulations of this work, RR scheme has converged without any relaxation, confirming its suitability for haemodynamics applications.

The results have been obtained with the parallel Finite Element library `LIFEV` developed at MOX - Politecnico di Milano, INRIA - Paris, CMCS - EPF of Lausanne and Emory University - Atlanta. The management of the parallelism relies on `ParMETIS` (http://glaros.dtc.umn.edu/
gkhome/views/metis), whilst the solution of the linear system on `Trilinos` (http://trilinos.sandia.gov). In particular, the fluid and structure linear systems are solved with GMRes, whilst the harmonic extension with Coniugate Gradient, all preconditioned with an Additive Shwartz preconditioner of the package `Ifpack` of Trilinos. The simulations were run on a cluster at the consortium `CILEA` (www.cilea.it, Segrate, Milan, Italy), with a 2-ways nodes Intel Xeon3.16 Ghz QuadCore as CPU and 16GB of ram per node.

4.2 Definition of the temporal schemes

Here, we introduce the temporal schemes we have considered in the numerical simulations. For what concernes the BDF schemes, in Table 1 we collect the values of the parameters β_i and ξ_i characterizing the method with order $p = 1, 2, 3, 4$. In what follows, we refer to the BDF scheme of order q as *BDFq*.

Regarding the Newmark/theta-methods, in Table 2 we report the values of the parameters involved in the discretization, as a function of two parameters a_1 and a_2, which completely describe the method. We observe that for the approximation of the first order derivative just one parameter is needed. In

particular, for the fluid momentum equation, defining $\theta := a_2/a_1$, we obtain

$$\frac{\rho_f}{\theta\Delta t}\boldsymbol{u}_f^{n+1}+\rho_f((\boldsymbol{u}_f^{n+1}-\boldsymbol{u}_m^{n+1})\cdot\nabla)\boldsymbol{u}_f^{n+1}-\nabla\cdot\boldsymbol{T}_f^{n+1}=\boldsymbol{f}_f^{n+1}+\frac{\rho_f}{\theta\Delta t}\boldsymbol{u}_f^{n}+\left(\frac{1}{\theta}-1\right)\rho_f\boldsymbol{w}_f^{n}. \tag{16}$$

By noticing that $\rho_f\boldsymbol{w}_f^0+\rho_f((\boldsymbol{u}_f^0-\boldsymbol{u}_m^0)\cdot\nabla)\boldsymbol{u}_f^0-\nabla\cdot\boldsymbol{T}_f^0=\boldsymbol{f}_f^0$, we obtain from (16) with $n=0$

$$\frac{\rho_f}{\theta\Delta t}\boldsymbol{u}_f^1+\rho_f((\boldsymbol{u}_f^1-\boldsymbol{u}_m^1)\cdot\nabla)\boldsymbol{u}_f^1-\nabla\cdot\boldsymbol{T}_f^1=$$

$$=\boldsymbol{f}_f^1+\frac{\rho_f}{\theta\Delta t}\boldsymbol{u}_f^1-\left(\frac{1}{\theta}-1\right)\rho_f((\boldsymbol{u}_f^0-\boldsymbol{u}_m^0)\cdot\nabla)\boldsymbol{u}_f^0+\left(\frac{1}{\theta}-1\right)\nabla\cdot\boldsymbol{T}_f^0+\left(\frac{1}{\theta}-1\right)\boldsymbol{f}_f^0,$$

and for a general step n, we recognize the theta-method

$$\frac{\rho_f}{\Delta t}\boldsymbol{u}_f^{n+1}+\theta\rho_f((\boldsymbol{u}_f^{n+1}-\boldsymbol{u}_m^{n+1})\cdot\nabla)\boldsymbol{u}_f^{n+1}+(1-\theta)((\boldsymbol{u}_f^{n}-\boldsymbol{u}_m^{n})\cdot\nabla)\boldsymbol{u}_f^{n}-\theta\nabla\cdot\boldsymbol{T}_f^{n+1}-(1-\theta)\nabla\cdot\boldsymbol{T}_f^{n}$$

$$=\theta\boldsymbol{f}_f^{n+1}+(1-\theta)\boldsymbol{f}_f^{n}.$$

On the other side, by following similar steps, for the structure problem we obtain the *Newmark scheme* with parameters a_1 and a_2. In this work we consider the *Midpoint* scheme, that is $a_1=0.5$ and $a_2=0.25$, for the structure, and *Crank-Nicolson*, that is $\theta=0.5$, for the fluid.

4.3 Boundary conditions

In all the simulations of this section, for the harmonic extension and for the structure, we prescribe at the artificial sections normal homogeneous Dirichlet conditions and tangential homogeneous Neumann conditions, that is we let the domain to move freely in the tangential direction. Moreover, at the fluid inlet we prescribe a specific flow rate (detailed case by case) through the Lagrange multipliers method (see [28, 29]). At the outlet, we propose to use an absorbing boundary condition, obtained by following [11]. However, differently from [11], here we want to focus on a condition which relates implicitly the flow rate and the mean pressure. By introducing the characteristic variables W_1 and W_2 related to a reduced one-dimensional FSI problem [30] and by setting $W_2|_\Gamma=0$, we obtain an absorbing boundary condition at the outlet Γ, which corresponds to

$$Q=g(P)=4\gamma^*A(P)\left(A(P)^{1/4}-A_0^{1/4}\right)\quad\text{on }\Gamma, \tag{17}$$

where Q is the flow rate, A is the area related to the mean pressure P through the *algebraic law*

$$A=\left(\frac{(P-P_{ext})\sqrt{\pi}}{\tau(A)}+A_0^{1/2}\right)^2, \tag{18}$$

$\gamma=\sqrt{\frac{\tau(A)}{2\rho_f\sqrt{\pi}}}$, with P_{ext} the external pressure. We observe that the algebraic law (18) gives an implicit expression for the area A, since τ depends on A itself.

For this reason, we set $\tau^* = \tau(A^*)$ and $\gamma^* = \gamma(A^*)$, where A^* is a reference value, which eventually could be updated during iterations. It is known that the choice of avoiding any reflection is not physiological, since some of them could occur from the peripheral system. However, in absence of data concerning the downstream cardiovascular tree, the choice of imposing absorbing boundary conditions seems to be acceptable. By considering the following Taylor expansion of (17) around a reference value $\widehat{P}$

$$Q = g(\widehat{P}) + \left.\frac{\partial g}{\partial P}\right|_{P=\widehat{P}} (P - \widehat{P}) \quad \text{on } \Gamma,$$

and approximating the mean pressure with the mean normal stress, we obtain the following *defective resistance boundary condition* in the normal direction [31]

$$\frac{1}{|\Gamma|}\int_\Gamma (\boldsymbol{T}_f\,\boldsymbol{n})\cdot\boldsymbol{n}\,d\sigma - \widehat{R}\int_\Gamma \boldsymbol{u}\cdot\boldsymbol{n}\,d\sigma = \widehat{P} - \widehat{R}\,g(\widehat{P}) \quad \text{on } \Gamma,$$

where $\widehat{R} := \left(\left.\frac{\partial g}{\partial P}\right|_{P=\widehat{P}}\right)^{-1}$ is the *resistance*, corresponding to

$$\widehat{R} = \sqrt{\frac{\rho_f \tau^*}{2\sqrt{\pi}}}\left.\left(\frac{1}{5A(\widehat{P})^{3/4} - 4A_0^{1/4}A(\widehat{P})^{1/2}}\right)\right|_\Gamma.$$

A first very simple choice consists in choosing $\widehat{P} = P_{ext}$ at each time step, leading to

$$\frac{1}{|\Gamma|}\int_\Gamma (\boldsymbol{T}_f\,\boldsymbol{n})\cdot\boldsymbol{n}\,d\sigma - R_e\int_{\Gamma^n} \boldsymbol{u}\cdot\boldsymbol{n}\,d\sigma = P_{ext} \quad \text{on } \Gamma, \tag{19}$$

where $R_e = \sqrt{\frac{\rho_f\tau^0}{2\sqrt{\pi}}}\,\frac{1}{A_0^{3/4}}$, $\tau^0 = \tau(A_0)$. Notice that $g(P_{ext}) = 0$.

In the simulations presented in Sections 4.4.1 and 4.4.2, we consider condition (19) at the outlets, with $P_{ext} = 0\,mmHg$.

4.4 Comparison among different algorithms

In this section, we show the numerical results concerning the performance of the different algorithms proposed in Section 3.

4.4.1 Cylindrical domain

We consider the cylindrical geometry depicted in Figure 5, where the length is $L = 5\,cm$, the fluid domain radius $R = 0.5\,cm$ and the structure thickness $H_s = 0.1\,cm$. We prescribe the following flow rate Q_{in} at the inlet

$$Q_{in} = \begin{cases} 30\,\sin(25\pi t)\,, & t \le 0.04\,s, \\ 0 & 0.04\,s < t \le T, \end{cases}$$

where $T = 0.08\,s$. The space discretization parameter is $h = 0.1\,cm$ for the fluid mesh and $h = 0.025$ for the structure mesh. We have about 15000 d.o.f. for the fluid and about 9000 for the structure. As tolerances in criteria (12), (13) and (14) we use $\varepsilon_1 = \varepsilon_2 = 10^{-8}$ and $\varepsilon_3 = \varepsilon_4 = 10^{-9}$. We run all the simulations on 3 processors for the solution of the fluid problem and on 1 processor for the structure.

In the first set of simulations, we consider a global first order scheme, namely BDF1 for the fluid (that is *backward Euler*) and BDF1 for the structure (BDF1/BDF1). We remind that in this case GCIS-1 and GCIS-1-extrap schemes coincide. In Figure 2, we report a comparison of the solutions obtained with different methods, namely Double-loop, Single-loop, GCIS-1, GCIS-2, ICIS-1 and ICIS-2. In particular, we show the results at three different sections, Σ_1 located at $0.25\,cm$ from the inlet, Σ_2 at $2.50\,cm$ and Σ_3 at $4.75\,cm$. For each of the three blocks, we report the radial displacement η of a point at the FS intercae on Σ_j^0 (left), the flow rate $Q := \int_{\Sigma_j} \boldsymbol{u}_f \cdot \boldsymbol{n}\, d\sigma$ (middle) and the mean pressure $P := \frac{1}{|\Sigma_j|}\int_{\Sigma_j} p_f\, d\sigma$ (right). In the figures at the bottom a zoom around the peak instant is shown. These results show that there is a general agreement among all the solutions. By taking the solution obtained with Double-loop scheme as the reference one, and zooming the solutions around the peak instant, it is possible to see that GCIS-1 features slight errors for the displacement and the mean pressure, whilst ICIS-1 for the flow rate. In order to quantify these errors, in the following tables we report the relative errors by using the solution obtained with Double-loop scheme as the reference one. In particular, in Tab. 3 we report the quantity

$$\frac{\max_j |x^j_{DL} - x^j_*|}{\max_j |x^j_{DL}|} \tag{20}$$

at the peak instant, where x^j is one of the computed solutions at section Σ_j, namely the mean structure displacement η, the flow rate Q or the mean pressure P, DL stands for Double-loop and * stands for one of the other schemes.

In Table 4, we show the relative errors at the three sections Σ_1, Σ_2 and Σ_3, computed with

$$\frac{\|x^j_{DL} - x^j_*\|_{L^\infty(0,T)}}{\|x^j_{DL}\|_{L^\infty(0,T)}}, \quad j = 1, 2, 3. \tag{21}$$

From these results, we observe that Single-loop scheme gives, as expected, the same solution as Double-loop up to the tolerances chosen. Among the other schemes, GCIS-m schemes exhibit an excellent accuracy for any value of m, with an error in any case less than 0.5%. Moreover, we can observe that each external iteration reduces the error of about one order of magnitude. This shows that if convergence is reached in the internal (RR) loop, then it is not necessary to reach convergence also in the external loop, and just few (even one) external iterations are enough to obtain an accurate solution. For what concernes ICIS-n schemes, the errors are quite higher. In particular, ICIS-1 scheme features an

error up to 2%. Obviously, the accuracy improves with $n = 2, 3$, but in any case the errors are higher than the corresponding GCIS scheme. This means that for this kind of simulations, inspired by haemodynamic applications, it seems that the fulfillment of the interface continuity condition is more crucial than the treatment of the interface position.

In Table 5 we report the mean number of iterations over the different instants, in the external and in the internal loop, and the CPU time normalized with respect to that of Double-loop scheme. From these results, we observe that Single-loop scheme is more expensive than Double-loop scheme. This could be explained by the fact that for the latter scheme the matrices are assembled only about 7 times per time step (since in the internal loop the matrices are not updated), against almost 14 times in Single-loop scheme. Moreover, we notice that the GCIS-m schemes are very efficient, the CPU time being reduced up to 4 times with respect to Double-loop. This makes this family of schemes very appealing for applications, since they improve the CPU time with respect to classical schemes, without affecting considerably the accuracy. For example, GCIS-1 scheme features a relative error which is always less than 0.5% reducing the CPU time of a factor 4. To obtain an improvement of the accuracy, it is possibile to choose a GCIS-m scheme with $m > 1$, paying the price of a larger CPU time. For example, GCIS-2 scheme improves the accuracy (the error being less than 0.03%) with doubled CPU time with respect to GCIS-1 (however halving the effort with respect of Double-loop scheme). Finally, we observe that ICIS-n schemes are more expensive than GCIS-m schemes. In particular, the computational effort decreases when m increases, in contrast to GCIS-m schemes. Again, this should be due to the fact the at each external loop we have to re-assemble the matrices.

In order to have a precise computation of how the global CPU time is decomposed among the different operations for the solution of the FSI problem, in Table 6 we report the absolute and relative CPU time for the main operations (F fluid, S structure, H harmonic extension). A particular regard has to be given to the solution of the fluid problem. This has been done by applying GMRes to the Lagrange multiplier/Schur complement equation, leading to a modular algorithm requiring the solution of 3 Neumann fluid problems (see [29, 32]). However, in Double-loop and GCIS-m schemes it is enough to solve the second of the three fluid problems just once per external iteration, so that at each RR iteration we have to solve just 2 fluid problems.

In Tab. 7, we report the errors obtained by using the *Midpoint* scheme for the structure and the *Crank-Nicolson* scheme for the fluid. These results confirm the trend highlighted by the results of the first order simulations, in particular the lower accuracy of the ICIS schemes with respect to the GCIS ones. We also observe that GCIS-1-extrap is more accurate than GCIS-1. This is due to the second order extrapolations of the fluid domain quantities. The results at different sections and the CPU times lead to the same conclusions as for BDF1/BDF1, and therefore we have not included them here. Due to the

lower accuracy and efficiency of ICIS-n schemes shown by our results, we do not consider these methods in the next results.

Finally, we want to understand if, when considering high order methods for Double-loop and Single-loop schemes, a suitable extrapolation of the FS interface could improve the efficiency, by providing a better starting point and decresing consequently the number of external iterations. Observe that the solution does not change as we are acting only on the initial guess. In Table 8 we report the average number of iterations of such schemes with and without extrapolation of the FS interface from previous time steps. These results show that when considering extrapolation a slight improvement is observed for BDF2/BDF2 and no significative improvement in the efficiency is obtained for BDF3/BDF3, so we conclude that the extrapolation is not necessary for Double-loop and Single-loop schemes.

4.4.2 Carotid domain

In this section we show the numerical results obtained in a real geometry of a human carotid. The aim here is to compare three of the methods described in the previous section, namely Double-loop, CGIS-1 and GCIS-2. In particular, at the inlet we prescribe the physiological flow-rate depicted in Figure 3. As tolerances in criteria (12), (13) and (14) we use $\varepsilon_1 = \varepsilon_2 = 10^{-7}$ and $\varepsilon_3 = \varepsilon_4 = 10^{-8}$. We consider BDF1/BDF1. We run the simulations on 15 processors for the solution of the fluid problem and on 1 processor for the structure.

In Figure 4, we show the wall shear stress at the peak instant (systole) computed with the three methods. We observe an excellent agreement among the three solutions. Moreover, the CPU time of GCIS-1 scheme normalized over that of Double loop is 0.30, whilst that of GCIS-2 is 0.47. These results confirm the accuracy and efficiency of GCIS-1 and GCIS-2 also for real applications, and therefore suggest that these methods could be an effective choice in the context of patient-specific simulations.

5 Convergence with respect to time

In this section, we aim at studying the time convergence order of the proposed schemes. With this aim, in the next section we consider an analytical test case, whilst in Section 5.2 we show some numerical results.

5.1 An analytical test case

In this section, we propose an analytical solution for the FSI problem in a 3D geometry, with the aim at validating the methods previously introduced, by the comparison between the exact and the numerical solutions.

We consider a straight cylinder as fluid domain and the extrusion of its lateral surface with a given thickness as structure domain. Referring to Figure 5, we

consider the linear elastic law (15) to describe the structure. We consider the FSI problem (1), with $\mathcal{D} = 0$ and with

$$\widetilde{\boldsymbol{\eta}}_s = \bar{\boldsymbol{\eta}} \quad \text{on } \Sigma^0_{out}, \tag{22}$$

instead of $(1)_6$, where

$$\bar{\boldsymbol{\eta}} := \begin{bmatrix} x^0_{s,1}(\cos\theta - 1) - x^0_{s,2}\sin\theta + c_1, \\ x^0_{s,1}\sin\theta + x^0_{s,2}(\cos\theta - 1) + c_2, \\ c_3, \end{bmatrix}$$

for given functions of time $\theta(t)$ and $\boldsymbol{c}(t)$. Moreover, we consider the following other boundary conditions

$$\begin{cases} \boldsymbol{u}_f = \bar{\boldsymbol{u}} & \text{on } \Sigma^t_{f,1} \cup \Sigma^t_{f,2}, \\ \widetilde{\boldsymbol{\eta}}_s = \bar{\boldsymbol{\eta}} & \text{on } \Sigma^0_{s,1} \cup \Sigma^0_{s,2}, \\ \widetilde{\boldsymbol{\eta}}_m = \bar{\boldsymbol{\eta}} & \text{on } \Sigma^0_{f,1} \cup \Sigma^0_{f,2}, \end{cases} \tag{23}$$

where

$$\bar{\boldsymbol{u}} := \begin{cases} \dot\theta(c_2 - x_{f,2}) + \dot c_1, \\ \dot\theta(x_{f,1} - c_1) + \dot c_2, \\ \dot c_3, \end{cases}$$

and the initial conditions

$$\begin{cases} \boldsymbol{u}_f = \bar{\boldsymbol{u}} & \text{for } t = 0, \\ \widetilde{\boldsymbol{\eta}}_s = \bar{\boldsymbol{\eta}} & \text{for } t = 0, \\ \frac{\partial \widetilde{\boldsymbol{\eta}}_s}{\partial t} = \frac{\partial \bar{\boldsymbol{\eta}}}{\partial t} & \text{for } t = 0. \end{cases} \tag{24}$$

Finally, we define the following forcing terms

$$\begin{aligned} \boldsymbol{f}_f &= \begin{cases} \rho_f \left(\dot\theta^2 (c_1 - x_{f,1}) + \ddot\theta (c_2 - x_{f,2}) + \ddot c_1 \right), \\ \rho_f \left(\dot\theta^2 (c_2 - x_{f,2}) + \ddot\theta (x_{f,1} - c_1) + \ddot c_2 \right), \\ \rho_f \ddot c_3, \end{cases} \\ \widetilde{\boldsymbol{f}}_s &= \begin{cases} -\rho_s \left(\ddot\theta \left(x^0_{s,1}\sin\theta + x^0_{s,2}\cos\theta \right) + \dot\theta^2 \left(x^0_{s,1}\cos\theta - x^0_{s,2}\sin\theta \right) - \ddot c_1 \right), \\ \rho_s \left(\ddot\theta \left(x^0_{s,1}\cos\theta - x^0_{s,2}\sin\theta \right) - \dot\theta^2 \left(x^0_{s,1}\sin\theta - x^0_{s,2}\cos\theta \right) - \ddot c_2 \right), \\ \rho_s \ddot c_3. \end{cases} \end{aligned} \tag{25}$$

It is easy to check that the analytical solution of $(1)_{1-5}$,(22), (23), (24) and (25) is given by

$$\begin{cases} \boldsymbol{u}_f = \bar{\boldsymbol{u}} & \text{in } \Omega^t_f, \\ p_f = \frac{E}{1+\nu} \left(1 + \frac{2\nu}{1-2\nu} \right) (1 - \cos(\theta)) & \text{in } \Omega^t_f, \\ \widetilde{\boldsymbol{\eta}}_s = \bar{\boldsymbol{\eta}} & \text{in } \Omega^0_s, \\ \widetilde{\boldsymbol{\eta}}_m = \bar{\boldsymbol{\eta}} & \text{in } \Omega^0_f. \end{cases}$$

This analytical solution represents a roto-translation of the points of the fluid-structure domain, that is $\boldsymbol{x}^t_f = R(t)\boldsymbol{x}^0_f + \boldsymbol{c}(t)$, where

$$R(t) := \begin{bmatrix} \cos\theta & -\sin\theta & 0 \\ \sin\theta & \cos\theta & 0 \\ 0 & 0 & 1 \end{bmatrix}$$

represents the rotation, and $\boldsymbol{c}(t)$ is the vector representing the translation.

5.2 Numerical results

The geometrical properties of the domain are the same of that in Section 4.4.1, whilst the numerical parameters are $h = 0.05\,cm$ for the fluid mesh and $0.015\,cm$ for the structure mesh. For what concernes the data of the test, we have set $\boldsymbol{c} = \mathbf{0}$ and $\theta(t) = 0.2(1 - cos(50\pi\, t))$. As tolerances in criteria (12), (13) and (14) we use $\varepsilon_1 = \varepsilon_2 = 10^{-7}$ and $\varepsilon_3 = \varepsilon_4 = 10^{-8}$. We run all the simulations on 31 processors for the solution of the fluid problem and on 1 processor for the structure.

In Figure 6 we show the convergence history of three selected temporal schemes, namely BDF1/BDF1, BDF2/BDF2, Midpont/Crank-Nicolson, whilst in Figure 7 the convergence hystory of BDF3/BDF3 and BDF4/BDF4. A relative L^2 norm is computed at time $t = 0.002\,s$ for the first four schemes, whilst at $t = 0.001\,s$ for BDF4/BDF4. The time discretization parameter is $\Delta t = 2 \cdot 10^{-3}$, 10^{-3}, $5 \cdot 10^{-4}$, $2.5 \cdot 10^{-4}\,s$ for the first four schemes, whilst we set $\Delta t = 10^{-3}$, $5 \cdot 10^{-4}$, $3.3 \cdot 10^{-4}$, $2.5 \cdot 10^{-4}\,s$ for BDF4/BDF4. These results show that the expected convergence orders are achieved for Double-loop and Single-loop scheme. We observe that for BDF4/BDF4, the fluid velocity and structure displacement errors' behaviour moves away from fourth order. This is probably due to the presence of the spatial error. GCIS-1 scheme is as expected first order accurate, whilst GCIS-1-extrap scheme allows to recover order q, showing that an extrapolation of order q of the FS interface and convective term is suitable to recover the right convergence order when performing just one external iteration. Moreover, when a m-th order discretization is considered, $m \geq 2$, GCIS-m schemes recover order m without any extrapolation. This is the reason why we have not considered GCIS-m-extrap schemes with $m \geq 2$ in this work. More interestingly, when a q-th order discretization is considered, GCIS-2 recover order q without any extrapolation even for $q = 3$ or $q = 4$.

6 Conclusions

In this work we considered the numerical solution of the FSI problem in haemodynamics with partitioned schemes. We started from a suitable formulation of the monolithic system and we derived solution schemes as quasi-Newton preconditioners. Among them, we considered several approaches: Double-Loop, Single-Loop, GCIS-m, ICIS-n, as well as a purely geometry explcit scheme GCIS-1-extrap with a $q - th$ order extrapolation of the interface position as well as the fluid convective term. We summarize in what follows the conclusion we

have drawn from the numerical solutions. In particular, for what concernes the efficiency of the schemes, we found that

1. Among the implicit schemes, Single-loop is less efficient than Double-loop;
2. An extrapolation of order q of geometrical quantites and convective term when using a $q-th$ order method does not improve the efficiency of Double-loop and Single-loop;
3. GCIS-m schemes provide an accurate solution also for $m = 1$ or $m = 2$, improving the efficiency with respect to Double-loop up to five and two times, respectively.

We also studied the accuracy with respect to time of the proposed schemes, by considering a new analytical test case for FSI problems, and by applying temporal schemes of order q both for the fluid and for the structure subproblems. We found that

4. Implicit schemes, as expected, recover globally a q-th order scheme;
5. GCIS-1 needs a $q-th$ order extrapolation of interface geometrical quantities and of fluid convective term to recover globally a $q-th$ order scheme. Without any extrapolation it is as expected first order accurate;
6. For GCIS-m, $m \geq 2$, no extrapolation is needed to recover a global order m. Moreover, we noticed that GCIS-2 recovers also order 3 and 4 when using BDF3/BDF3 or BDF4/BDF4, respectively, *without any extrapolation*.

In conclusion, we can state that GCIS-2 seems to be a very effective scheme for the solution of FSI problems in haemodynamics for clinical purposes. The next step is to check its accuracy and efficiency also when a non-linear structure is considered.

Acknowledgements

The authors have been partially supported by the ERC Advanced Grant N.227058 MATHCARD.

References

[1] Perktold K, Thurner E, Kenner T. Flow and stress characteristics in rigid walled and compliant carotid artery bifurcation models. *Medical and Biological Engineering and Computing* 1994; **32**(1):19–26.

[2] Bazilevs Y, Calo V, Zhang Y, Hughes T. Isogeometric fluid-structure interaction analysis with applications to arterial blood flow. *Computational Mechanics* 2006; **38**:310–322.

[3] Figueroa C, Vignon-Clementel I, Jansen K, Hughes T, Taylor C. A coupled momentum method for modeling blood flow in three-dimensional deformable arteries. *Computer Methods in Applied Mechanics and Engineering* 2006; **195**:5685–5706.

[4] Tezduyar T, Sathe S, Cragin T, Nanna B, Conklin B, Pausewang J, Schwaab M. Modelling of fluid-structure interactions with the space-time finite elements: arterial fluid mechanics. *International Journal for Numerical Methods in Fluids* 2007; **54**:901–922.

[5] Badia S, Nobile F, Vergara C. Fluid-structure partitioned procedures based on Robin transmission conditions. *Journal of Computational Physics* 2008; **227**:7027–7051.

[6] Formaggia L, Quarteroni A, (Eds) AV. *Cardiovascular Mathematics - Modeling and simulation of the circulatory system*. Springer, 2009.

[7] Heil M. An efficient solver for the fully coupled solution of large-displacement fluid-structure interaction problems. *Computer Methods in Applied Mechanics and Engineering* 2004; **193**:1–23.

[8] Fernández M, Moubachir M. A Newton method using exact Jacobians for solving fluid-structure coupling. *Computers & Structures* 2005; **83(2-3)**:127–142.

[9] Fernández M, Gerbeau J, Grandmont C. A projection semi-implicit scheme for the coupling of an elastic structure with an incompressible fluid. *International Journal for Numerical Methods in Engineering* 2007; **69**(4):794–821.

[10] Badia S, Quaini A, Quarteroni A. Splitting methods based on algebraic factorization for fluid-structure interaction. *SIAM J Sc Comp* 2008; **30**(4):1778–1805.

[11] Nobile F, Vergara C. An effective fluid-structure interaction formulation for vascular dynamics by generalized Robin conditions. *SIAM J Sc Comp* 2008; **30**(2):731–763.

[12] Crosetto P, Deparis S, Fourestey G, Quarteroni A. Parallel algorithms for fluid-structure interaction problems in haemodynamics. *EPFL-REPORT-148536* 2009; .

[13] Gee M, Kuttler U, Wall W. Truly monolithic algebraic multigrid for fluid-structure interaction. *International Journal for Numerical Methods in Engineering* 2011; **85(8)**:987–1016.

[14] Piperno S, Farhat C. Design of efficient partitioned procedures for transient solution of aerolastic problems. *Rev. Eur. Elements Finis* 2000; **9(6-7)**:655–680.

[15] Causin P, Gerbeau J, Nobile F. Added-mass effect in the design of partitioned algorithms for fluid-structure problems. *Computer Methods in Applied Mechanics and Engineering* 2005; **194(42-44)**:4506–4527.

[16] Deparis S, Discacciati M, Fourestey G, Quarteroni A. Fluid-structure algorithms based on Steklov-Poincaré operators. *Computer Methods in Applied Mechanics and Engineering* 2006; **195**(41-43):5797–5812.

[17] Forster C, Wall W, Ramm E. Artificial added mass instabilities in sequential staggered coupling of nonlinear structures and incompressible viscous flow. *Computer Methods in Applied Mechanics and Engineering* 2007; **196**(7):1278–1293.

[18] Hughes TJR, Liu WK, Zimmermann TK. Lagrangian-Eulerian finite element formulation for incompressible viscous flows. *Computer Methods in Applied Mechanics and Engineering* 1981; **29**(3):329–349.

[19] Donea J. An arbitrary Lagrangian-Eulerian finite element method for transient dynamic fluid-structure interaction. *Computer Methods in Applied Mechanics and Engineering* 1982; **33**:689–723.

[20] Nobile F. Numerical approximation of fluid-structure interaction problems with application to haemodynamics. PhD Thesis, École Polytechnique Fédérale de Lausanne 2001. Thesis n° 2458.

[21] Moireau P, Xiao N, Astorino M, Figueroa CA, Chapelle D, Taylor CA, Gerbeau JF. External tissue support and fluidstructure simulation in blood flows. *Biomechanics and Modeling in Mechanobiology* 2011; doi:DOI 10.1007/s10237-011-0289-z.

[22] Liu Y, Charles C, Gracia M, Gregersen H, Kassab GS. Surrounding tissues affect the passive mechanics of the vessel wall: theory and experiment. *Am J Physiol Heart Circ Physiol* 2007; **293**:H3290–H3300.

[23] Hairer E, Nørsett S, Wanner G. *Solving ordinary differential equations: Nonstiff problems*. Springer series in computational mathematics, Springer, 1993.

[24] Hairer E, Wanner G. *Solving Ordinary Differential Equations II: Stiff and Differential-Algebraic Problems*. Springer Series in Computational Mathematics, Springer, 2010.

[25] Badia S, Nobile F, Vergara C. Robin-Robin preconditioned Krylov methods for fluid-structure interaction problems. *Computer Methods in Applied Mechanics and Engineering* 2009; **198**(33-36):2768–2784.

[26] Astorino M, Chouly F, Fernández M. Robin based semi-implicit coupling in fluid-structure interaction: stability analysis and numerics. *SIAM J Sc Comp* 2009; (31(6)):4041–4065.

[27] Giorda LG, Nobile F, Vergara C. Analysis and optimization of robin-robin partitioned procedures in fluid-structure interaction problems. *SIAM Journal on Numerical Analysis* 2010; **48(6)**:2091–2116.

[28] Formaggia L, Gerbeau JF, Nobile F, Quarteroni A. Numerical treatment of defective boundary conditions for the Navier-Stokes equation. *SIAM Journal on Numerical Analysis* 2002; **40(1)**:376–401.

[29] Veneziani A, Vergara C. Flow rate defective boundary conditions in haemodinamics simulations. *International Journal for Numerical Methods in Fluids* 2005; **47**:803–816.

[30] Formaggia L, Gerbeau JF, Nobile F, Quarteroni A. On the coupling of 3D an 1D Navier-Stokes equations for flow problems in compliant vessels. *Computer Methods in Applied Mechanics and Engineering* 2001; **191(6-7)**:561–582.

[31] Vergara C. Nitsches method for defective boundary value problems in incompressibile fluid-dynamics. *J Sci Comp* 2011; **46(1)**:100–123.

[32] Formaggia L, Veneziani A, Vergara C. Flow rate boundary problems for an incompressible fluid in deformable domains: formulations and solution methods. *Computer Methods in Applied Mechanics and Engineering* 2009; **199 (9-12)**:677–688.

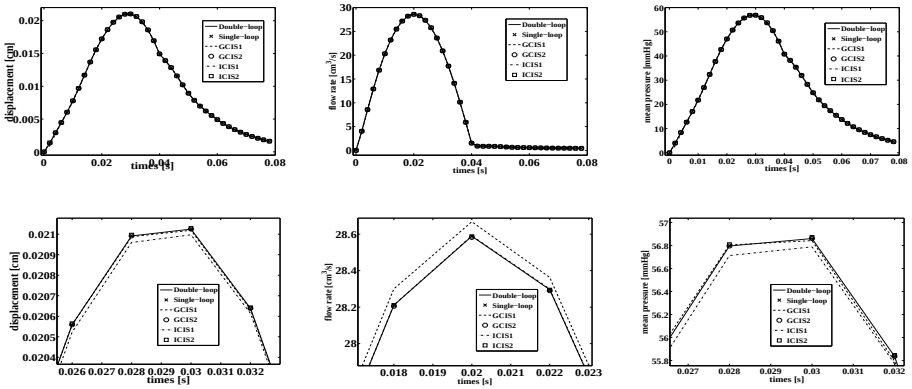

(a) Solutions at section Σ_1

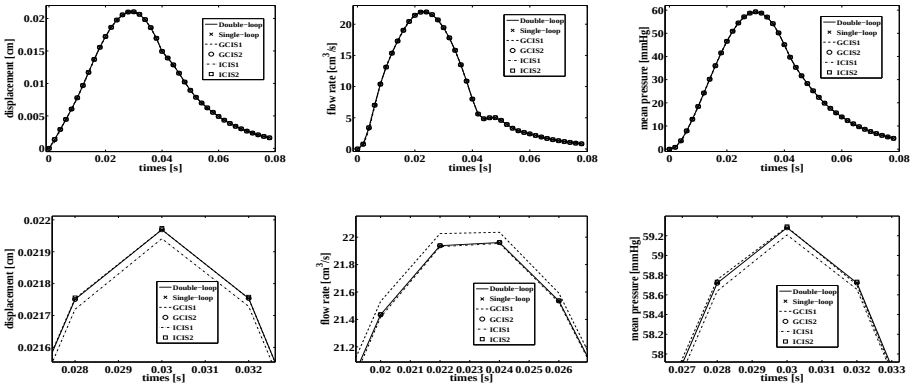

(b) Solutions at section Σ_2

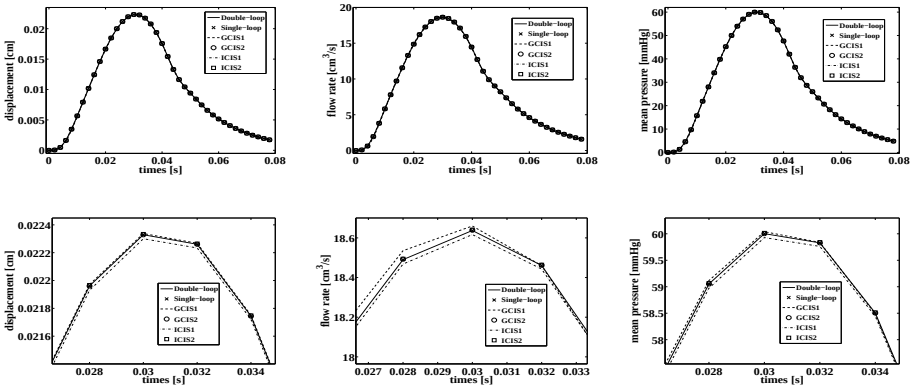

(c) Solutions at section Σ_3

Figure 2: For each of the three blocks, the comparison of the solution obtained with different schemes is reported (up: whole interval, bottom: a zoom around the peak instant). Displacement (left), flow rate (middle), mean pressure (right) - BDF1-BDF1.

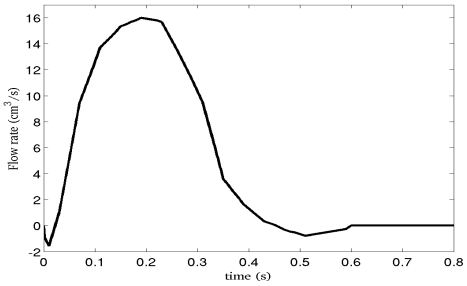

Figure 3: Flow rate waveform prescribed at the inlet of the carotid.

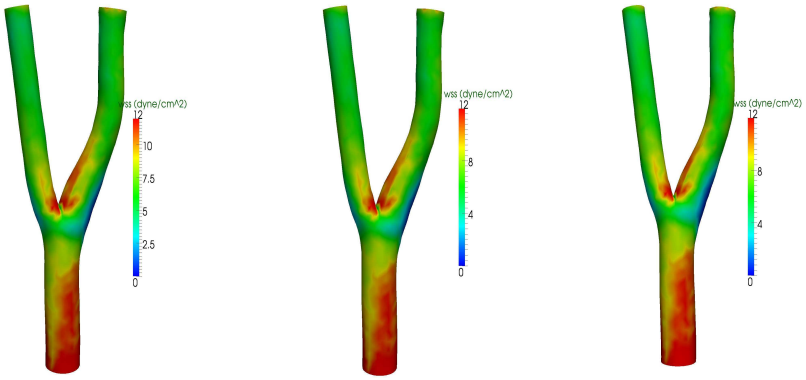

Figure 4: Wall shear stress at the systole computed with Double loop (left), GCIS-1 (middle) and GCIS-2 (right).

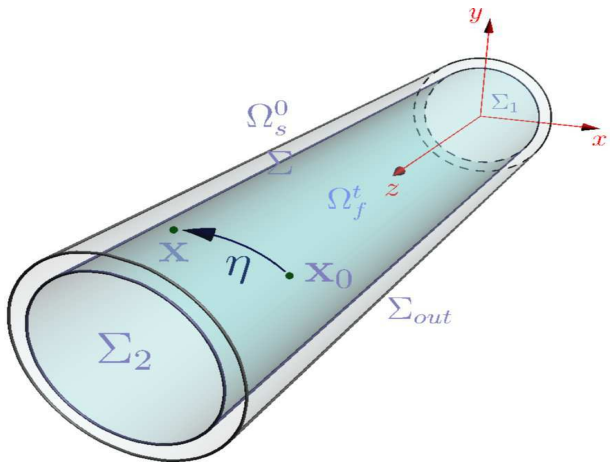

Figure 5: Geometry in the test case.

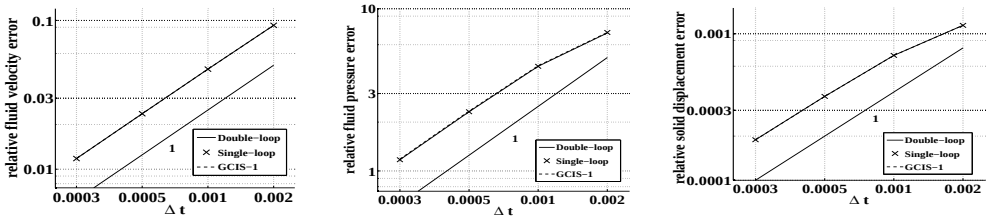

(a) BDF1/BDF1

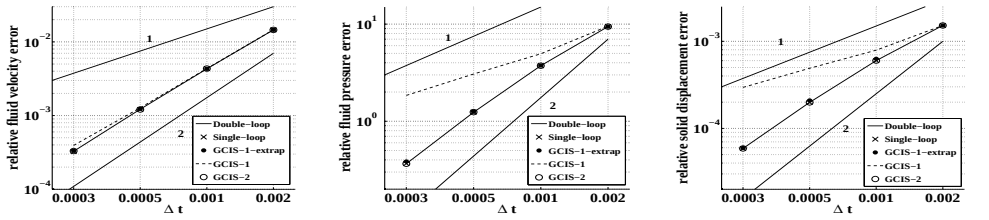

(b) BDF2/BDF2

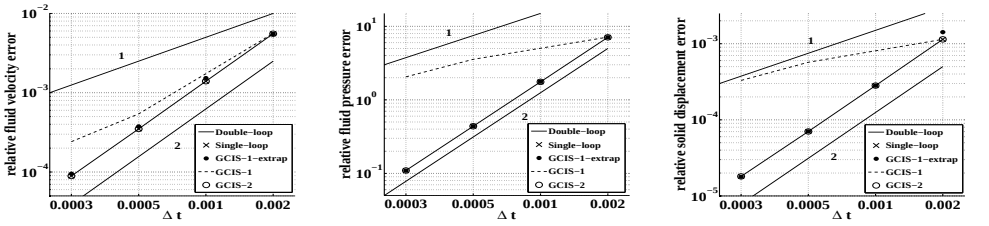

(c) Midpoint/Crank-Nicolson

Figure 6: Convergence rate of three schemes considered. Relative errors of the fluid velocity (left), of the pressure (middle) and of the structure displacement (right) - BDF1/BDF1 (up), BDF2/BDF2 (middle), Midpoint/Crank-Nicolson (bottom) - $t = 0.002\,s$.

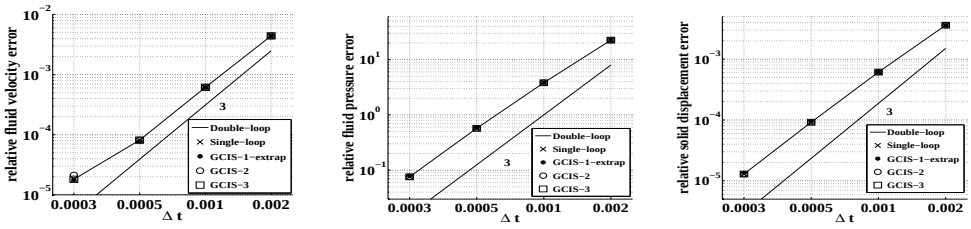

(a) BDF3/BDF3

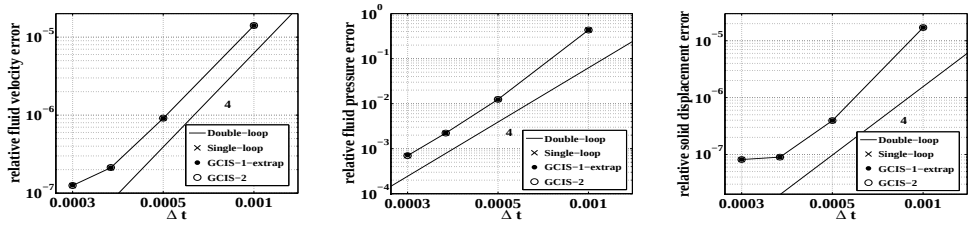

(b) BDF4/BDF4

Figure 7: Convergence rate of two schemes considered. Relative errors of the fluid velocity (left), of the pressure (middle) and of the structure displacement (right) - BDF3/BDF3 - $t = 0.002\,s$ (up), BDF4/BDF4 - $t = 0.001\,s$ (bottom).

Tables

	β_0	β_1	β_2	β_3	β_4	ξ_0	ξ_1	ξ_2	ξ_3	ξ_4	ξ_5
1	1	1	–	–	–	1	2	-1	–	–	–
2	3/2	2	-1/2	–	–	2	5	-4	1	–	–
3	11/6	3	-3/2	1/3	–	35/12	26/3	-19/2	14/3	-11/12	–
4	25/12	4	-3	4/3	-1/4	15/4	77/6	-107/6	13	-61/12	5/6

Table 1: Values of the parameters β_i and ξ_i for the BDF schemes for the approximation of first and second derivatives, respectively - $p = 1, 2, 3, 4$.

$\beta_0 = \beta_1$	χ	κ	$\xi_0 = \xi_1 = \sigma$	ζ
$\frac{a_1}{a_2}$	$\frac{a_1}{a_2} - 1$	$\frac{a_1}{2a_2} - 1$	$\frac{1}{a_2}$	$\frac{1}{2a_2} - 1$

Table 2: Values of the parameters involved in the discretization with Newmark/theta-methods.

	η (%)	Q (%)	P(%)
Single loop	0.0006	0.0004	0.0002
GCIS-1	0.0845	0.3563	0.2548
GCIS-2	0.0023	0.0220	0.0008
GCIS-3	0.0001	0.0004	0.0001
ICIS-1	0.3263	0.1532	0.3122
ICIS-2	0.0538	0.0250	0.0517
ICIS-3	0.0110	0.0051	0.0102

Table 3: Relative error with respect to Double-loop scheme, computed with (20). BDF1/BDF1. Left: displacement. Middle: flow rate. Right: mean pressure. Peak instant $t = 0.02\,s$.

	Section Σ_1			Section Σ_2			Section Σ_3		
	η (%)	Q (%)	P (%)	η (%)	Q (%)	P (%)	η (%)	Q (%)	P (%)
Single loop	0.0053	0.0168	0.0098	0.0009	0.0026	0.0009	0.0009	0.0011	0.0009
GCIS-1	0.1415	0.3316	0.2347	0.1182	0.4607	0.2076	0.1168	0.4893	0.1946
GCIS-2	0.0014	0.0224	0.0015	0.0005	0.0014	0.0010	0.0018	0.0172	0.0005
GCIS-3	0.0005	0.0026	0.0002	0.0001	0.0005	0.0002	0.0004	0.0005	0.0002
ICIS-1	1.8054	0.6214	1.9935	0.7582	1.8147	0.7850	0.8098	0.9652	0.8335
ICIS-2	0.2786	0.0446	0.3050	0.1322	0.3043	0.1381	0.1420	0.1705	0.1467
ICIS-3	0.0365	0.0030	0.0398	0.0225	0.0319	0.0246	0.0217	0.0249	0.0225

Table 4: Relative error with respect to Double-loop scheme, computed with (21), at three different sections. BDF1/BDF1.

	# of external iterations	# of internal iterations	Normalized CPU time
Double-loop	7.1	5.2	1.00
Single-loop	13.7	-	1.13
GCIS-1	1.0	14.3	0.23
GCIS-2	2.0	12.0	0.45
GCIS-3	3.0	9.7	0.60
ICIS-1	12.9	1.0	1.11
ICIS-2	8.7	1.8	0.75
ICIS-3	7.1	2.7	0.69

Table 5: Average number of iterations in the external and in the internal loop (for Single-loop the only loop is indicated as external) and CPU time normalized with respect to that of Double-loop scheme. BDF1/BDF1.

Loop	Operation	CPU time (s)	(%)
External loop	H assemble rhs and solve	0.02	0.2
	F assemble matrices	4.23	45.0
	F compute preconditioner	1.95	20.1
	F assemble rhs	0.17	1.8
	F solve	1.13	12.0
Internal loop	F assemble rhs	0.34	3.6
	F solve	1.30	13.8
	S assemble rhs	0.20	2.1
	S solve	0.05	0.5

Table 6: Decomposition of the CPU time for the main operations in the solution of the FSI problem. The relative times (right coloumn) refer to the sum of the operations needed to perform one external and one internal loop.

	η (%)	Q (%)	P (%)
Single loop	0.0023	0.0055	0.0029
GCIS-1	0.0794	0.0617	0.0531
GCIS-1-extrap	0.0321	0.0254	0.0213
GCIS-2	0.0315	0.0171	0.0208
GCIS-3	0.0012	0.0051	0.0008
ICIS-1	1.2922	1.0162	1.1740
ICIS-2	0.0405	0.0547	0.0315
ICIS-3	0.0130	0.0104	0.0153

Table 7: Relative error with respect to Double-loop scheme, computed with (20). Midpoint/Crank-Nicolson. Left: displacement. Middle: flow rate. Right: mean pressure. Peak instant $t = 0.02\,s$.

	BDF1	BDF2	BDF3
Single-loop	13.7	16.7	14.7
Single-loop-extrap	-	14.6	14.6
Double loop	7.1	7.6	6.7
Double-loop-extrap	-	6.2	6.5

Table 8: Average number of iterations (in the external loop for Double loop).